JHEP

Published for SISSA by Springer

Received: December 9, 2011
Accepted: June 24, 2012
Published: July 18, 2012

Underlying Event measurements in pp collisions at $\sqrt{s} = 0.9$ and 7 TeV with the ALICE experiment at the LHC

The ALICE collaboration

E-mail: jgrosseo@cern.ch

Abstract: We present measurements of Underlying Event observables in pp collisions at $\sqrt{s} = 0.9$ and 7 TeV. The analysis is performed as a function of the highest charged-particle transverse momentum $p_{\mathrm{T,LT}}$ in the event. Different regions are defined with respect to the azimuthal direction of the leading (highest transverse momentum) track: Toward, Transverse and Away. The Toward and Away regions collect the fragmentation products of the hardest partonic interaction. The Transverse region is expected to be most sensitive to the Underlying Event activity. The study is performed with charged particles above three different p_{T} thresholds: 0.15, 0.5 and 1.0 GeV/c. In the Transverse region we observe an increase in the multiplicity of a factor 2–3 between the lower and higher collision energies, depending on the track p_{T} threshold considered. Data are compared to Pythia 6.4, Pythia 8.1 and Phojet. On average, all models considered underestimate the multiplicity and summed p_{T} in the Transverse region by about 10–30%.

Keywords: Hadron-Hadron Scattering

ArXiv ePrint: 1112.2082

doi:10.1007/JHEP07(2012)116

JHEP07(2012)116

Contents

JHEP07(2012)116

1 Introduction

The detailed characterization of hadronic collisions is of great interest for the understanding of the underlying physics. The production of particles can be classified according to the energy scale of the process involved. At high transverse momentum transfers ($p_{\mathrm{T}} \gtrsim 2\,\mathrm{GeV}/c$) perturbative Quantum Chromodynamics (pQCD) is the appropriate theoretical framework to describe partonic interactions. This approach can be used to quantify parton yields and correlations, whereas the transition from partons to hadrons is a non-perturbative process that has to be treated using phenomenological approaches. Moreover, the bulk of particles produced in high-energy hadronic collisions originate from low-momentum transfer processes. For momenta of the order of the QCD scale, $\mathcal{O}(100\,\mathrm{MeV})$, a perturbative treatment is no longer feasible. Furthermore, at the center-of-mass energies of the Large Hadron Collider (LHC), at momentum transfers of a few GeV/c, the calculated QCD cross-sections for 2-to-2 parton scatterings exceed the total hadronic cross-section [1]. This result indicates that Multiple Partonic Interactions (MPI) occur in this regime. The overall event dynamics cannot be derived fully from first principles and must be modeled using phenomenological

calculations. Measurements at different center-of-mass energies are required to test and constrain these models.

In this paper, we present an analysis of the bulk particle production in pp collisions at the LHC by measuring the so-called Underlying Event (UE) activity [2]. The UE is defined as the sum of all the processes that build up the final hadronic state in a collision excluding the hardest leading order partonic interaction. This includes fragmentation of beam remnants, multiple parton interactions and initial- and final-state radiation (ISR/FSR) associated to each interaction. Ideally, we would like to study the correlation between the UE and perturbative QCD interactions by isolating the two leading partons with topological cuts and measuring the remaining event activity as a function of the transferred momentum scale (Q^2). Experimentally, one can identify the products of the hard scattering, usually the leading jet, and study the region azimuthally perpendicular to it as a function of the jet energy. Results of such an analysis have been published by the CDF [2–5] and STAR [6] collaborations for pp collisions at $\sqrt{s} = 1.8$ and 0.2 TeV, respectively. Alternatively, the energy scale is given by the leading charged-particle transverse momentum, circumventing uncertainties related to the jet reconstruction procedure at low p_{T}. It is clear that this is only an approximation to the original outgoing parton momentum, the exact relation depends on the details of the fragmentation mechanism. The same strategy based on the leading charged particle has recently been applied by the ATLAS [7] and CMS [8] collaborations.

In the present paper we consider only charged primary particles,[1] due to the limited calorimetric acceptance of the ALICE detector systems in azimuth. Distributions are measured for particles in the pseudorapidity range $|\eta| < 0.8$ with $p_{\mathrm{T}} > p_{\mathrm{T,min}}$, where $p_{\mathrm{T,min}} = 0.15$, 0.5 and 1.0 GeV/$c$, and are studied as a function of the leading particle transverse momentum.

Many Monte Carlo (MC) generators for the simulation of pp collisions are available; see [9] for a recent review discussing for example Pythia [10], Phojet [11], Sherpa [9] and Herwig [12]. These provide different descriptions of the UE associated with high energy hadron collisions. A general strategy is to combine a perturbative QCD treatment of the hard scattering with a phenomenological approach to soft processes. This is the case for the two models used in our analysis: Pythia and Phojet. In Pythia the simulation starts with a hard LO QCD process of the type $2 \to 2$. Multi-jet topologies are generated with the parton shower formalism and hadronization is implemented through the Lund string fragmentation model [13]. Each collision is characterized by a different impact parameter b. Small b values correspond to a large overlap of the two incoming hadrons and to an increased probability for MPIs. At small p_{T} values color screening effects need to be taken into account. Therefore a cut-off $p_{\mathrm{T,0}}$ is introduced, which damps the QCD cross-section for $p_{\mathrm{T}} \ll p_{\mathrm{T,0}}$. This cut-off is one of the main tunable model parameters.

In Pythia version 6.4 [10] MPI and ISR have a common transverse momentum evolution scale (called interleaved evolution [14]). Version 8.1 [15] is a natural extension of version 6.4, where the FSR evolution is interleaved with MPI and ISR and parton rescat-

[1] Primary particles are defined as prompt particles produced in the collision and their decay products (strong and electromagnetic decays), except products of weak decays of strange particles such as K^0_S and Λ.

JHEP07(2012)116

terings [16] are considered. In addition initial-state partonic fluctuations are introduced, leading to a different amount of color-screening in each event.

PHOJET is a two-component event generator, where the soft regime is described by the Dual Parton Model (DPM) [17] and the high-p_{T} particle production by perturbative QCD. The transition between the two regimes happens at a p_{T} cut-off value of 3 GeV/c. A high-energy hadronic collision is described by the exchange of effective Pomerons. Multiple-Pomeron exchanges, required by unitarization, naturally introduce MPI in the model.

UE observables allow one to study the interplay of the soft part of the event with particles produced in the hard scattering and are therefore good candidates for Monte Carlo tuning. A better understanding of the processes contributing to the global event activity will help to improve the predictive power of such models. Further, a good description of the UE is needed to understand backgrounds to other observables, e.g., in the reconstruction of high-p_{T} jets.

The paper is organized in the following way: the ALICE sub-systems used in the analysis are described in section 2 and the data samples in section 3. Section 4 is dedicated to the event and track selection. Section 5 introduces the analysis strategy. In sections 6 and 7 we focus on the data correction procedure and systematic uncertainties, respectively. Final results are presented in section 8 and in section 9 we draw conclusions.

2 ALICE detector

Optimized for the high particle densities encountered in heavy-ion collisions, the ALICE detector is also well suited for the study of pp interactions. Its high granularity and particle identification capabilities can be exploited for precise measurements of global event properties [18–24]. The central barrel covers the polar angle range $45° - 135°$ ($|\eta| < 1$) and full azimuth. It is contained in the L3 solenoidal magnet which provides a nominal uniform magnetic field of 0.5 T. In this section we describe only the trigger and tracking detectors used in the analysis, while a detailed discussion of all ALICE sub-systems can be found in [25].

The V0A and V0C counters consist of scintillators with a pseudorapidity coverage of $-3.7 < \eta < -1.7$ and $2.8 < \eta < 5.1$, respectively. They are used as trigger detectors and to reject beam-gas interactions.

Tracks are reconstructed combining information from the two main tracking detectors in the ALICE central barrel: the Inner Tracking System (ITS) and the Time Projection Chamber (TPC). The ITS is the innermost detector of the central barrel and consists of six layers of silicon sensors. The first two layers, closely surrounding the beam pipe, are equipped with high granularity Silicon Pixel Detectors (SPD). They cover the pseudorapidity ranges $|\eta| < 2.0$ and $|\eta| < 1.4$ respectively. The position resolution is 12 μm in $r\phi$ and about 100 μm along the beam direction. The next two layers are composed of Silicon Drift Detectors (SDD). The SDD is an intrinsically 2-dimensional sensor. The position along the beam direction is measured via collection anodes and the associated resolution is about 50 μm. The $r\phi$ coordinate is given by a drift time measurement with a spatial resolution of about 60 μm. Due to drift field non-uniformities, which were not corrected for in the 2010 data, a systematic uncertainty of 300 μm is assigned to the SDD points. Finally, the two outer layers are made of double-sided Silicon micro-Strip Detectors (SSD) with a position

JHEP07(2012)116

resolution of 20 μm in $r\phi$ and about 800 μm along the beam direction. The material budget of all six layers including support and services amounts to 7.7% of a radiation length.

The main tracking device of ALICE is the Time Projection Chamber that covers the pseudorapidity range of about $|\eta| < 0.9$ for tracks traversing the maximum radius. In order to avoid border effects, the fiducial region has been restricted in this analysis to $|\eta| < 0.8$. The position resolution along the $r\phi$ coordinate varies from 1100 μm at the inner radius to 800 μm at the outer. The resolution along the beam axis ranges from 1250 μm to 1100 μm.

For the evaluation of the detector performance we use events generated with the Pythia 6.4 [10] Monte Carlo with tune Perugia-0 [26] passed through a full detector simulation based on Geant3 [27]. The same reconstruction algorithms are used for simulated and real data.

3 Data samples

The analysis uses two data sets which were taken at the center-of-mass energies of $\sqrt{s} =$ 0.9 and 7 TeV. In May 2010, ALICE recorded about 6 million good quality minimum-bias events at $\sqrt{s} = 0.9$ TeV. The luminosity was of the order of 10^{26} cm^{-2} s^{-1} and, thus, the probability for pile-up events in the same bunch crossing was negligible. The $\sqrt{s} =$ 7 TeV sample of about 25 million events was collected in April 2010 with a luminosity of 10^{27} cm^{-2} s^{-1}. In this case the mean number of interactions per bunch crossing μ ranges from 0.005 to 0.04. A set of high pile-up probability runs ($\mu = 0.2$–2) was analysed in order to study our pile-up rejection procedure and determine its related uncertainty. Those runs are excluded from the analysis.

Corrected data are compared to three Monte Carlo models: Pythia 6.4 (tune Perugia-0), Pythia 8.1 (tune 1 [15]) and Phojet 1.12.

4 Event and track selection

4.1 Trigger and offline event selection

Events are recorded if either of the three triggering systems, V0A, V0C or SPD, has a signal. The arrival time of particles in the V0A and V0C are used to reject beam-gas interactions that occur outside the nominal interaction region. A more detailed description of the online trigger can be found in [20]. An additional offline selection is made following the same criteria but considering reconstructed information instead of online trigger signals.

For each event a reconstructed vertex is required. The vertex reconstruction procedure is based on tracks as well as signals in the SPD. Only vertices within $\pm$10 cm of the nominal interaction point along the beam axis are considered. Moreover, we require at least one track with $p_{\mathrm{T}} > p_{\mathrm{T,min}} = 0.15$, 0.5 or 1.0 GeV/$c$ in the acceptance $|\eta| < 0.8$.

A pile-up rejection procedure is applied to the set of data taken at $\sqrt{s} = 7$ TeV: events with more than one distinct reconstructed primary vertex are rejected. This cut has a negligible effect on simulated events without pile-up: only 0.06% of the events are removed. We have compared a selection of high pile-up probability runs (see section 3) with a sample of low pile-up probability runs. The UE distributions differ by 20–25% between the two

JHEP07(2012)116

Collision energy: 0.9 TeV		
	Events	**% of all**
Offline trigger	5,515,184	100.0
Reconstructed vertex	4,482,976	81.3
Leading track $p_{\mathrm{T}} > 0.15$ GeV/c	4,043,580	73.3
Leading track $p_{\mathrm{T}} > 0.5$ GeV/c	3,013,612	54.6
Leading track $p_{\mathrm{T}} > 1.0$ GeV/c	1,281,269	23.2
Collision energy: 7 TeV		
	Events	**% of all**
Offline trigger	25,137,512	100.0
Reconstructed vertex	22,698,200	90.3
Leading track $p_{\mathrm{T}} > 0.15$ GeV/c	21,002,568	83.6
Leading track $p_{\mathrm{T}} > 0.5$ GeV/c	17,159,249	68.3
Leading track $p_{\mathrm{T}} > 1.0$ GeV/c	9,873,085	39.3

Table 1. Events remaining after each event selection step.

Selection criteria	**Value**
Detectors required	ITS,TPC
Minimum number of TPC clusters	70
Maximum χ^2 per TPC cluster	4
Minimum number of ITS clusters	3
Minimum number of SPD or 1^{st} layer SDD clusters	1
Maximum DCA_Z	2 cm
Maximum $DCA_{XY}(p_{\mathrm{T}})$	7σ

Table 2. Track selection criteria.

samples. After the above mentioned rejection procedure, the difference is reduced to less than 2%. Therefore, in the runs considered in the analysis, the effect of pile-up is negligible.

No explicit rejection of cosmic-ray events is applied since cosmic particles are efficiently suppressed by our track selection cuts [23]. This is further confirmed by the absence of a sharp enhanced correlation at $\Delta\phi = \pi$ from the leading track which would be caused by almost straight high-p_{T} tracks crossing the detector.

Table 1 summarizes the percentage of events remaining after each event selection step. We do not explicitly select non-diffractive events, although the above mentioned event selection significantly reduces the amount of diffraction in the sample. Simulated events show that the event selections reduce the fraction of diffractive events from 18–33% to 11–16% (Pythia 6.4 and Phojet at 0.9 and 7 TeV). We do not correct for this contribution.

JHEP07(2012)116

4.2 Track cuts

The track cuts are optimized to minimize the contamination from secondary tracks. For this purpose a track must have at least 3 ITS clusters, one of which has to be in the first 3 layers. Moreover, we require at least 70 (out of a maximum of 159) clusters in the TPC drift volume. The quality of the track fitting measured in terms of the χ^2 per space point is required to be lower than 4 (each space point having 2 degrees of freedom). We require the distance of closest approach of the track to the primary vertex along the beam axis (DCA_Z) to be smaller than 2 cm. In the transverse direction we apply a p_{T} dependent DCA_{XY} cut, corresponding to 7 standard deviations of its inclusive probability distribution. These cuts are summarized in table 2.

5 Analysis strategy

The Underlying Event activity is characterized by the following observables [2]:

- average charged particle density vs. leading track transverse momentum $p_{\mathrm{T,LT}}$:

$$\frac{1}{\Delta\eta \cdot \Delta\Phi} \frac{1}{N_{\mathrm{ev}}(p_{\mathrm{T,LT}})} N_{\mathrm{ch}}(p_{\mathrm{T,LT}}) \tag{5.1}$$

- average summed p_{T} density vs. leading track $p_{\mathrm{T,LT}}$:

$$\frac{1}{\Delta\eta \cdot \Delta\Phi} \frac{1}{N_{\mathrm{ev}}(p_{\mathrm{T,LT}})} \sum p_{\mathrm{T}}(p_{\mathrm{T,LT}}) \tag{5.2}$$

- $\Delta\phi$-correlation between tracks and the leading track:

$$\frac{1}{\Delta\eta} \frac{1}{N_{\mathrm{ev}}(p_{\mathrm{T,LT}})} \frac{\mathrm{d}N_{\mathrm{ch}}}{\mathrm{d}\Delta\phi} \tag{5.3}$$

  (in bins of leading track $p_{\mathrm{T,LT}}$).

N_{ev} is the total number of events selected and $N_{\mathrm{ev}}(p_{\mathrm{T,LT}})$ is the number of events in a given leading-track transverse-momentum bin. The first two variables are evaluated in three distinct regions. These regions, illustrated in figure 1, are defined with respect to the leading track azimuthal angle:

- Toward: $|\Delta\phi| < 1/3\ \pi$
- Transverse: $1/3\ \pi < |\Delta\phi| < 2/3\ \pi$
- Away: $|\Delta\phi| > 2/3\ \pi$

where $\Delta\phi = \phi_{LT} - \phi$ is defined in $\pm\pi$. In eq. (5.1)–(5.3) the normalization factor $\Delta\Phi$ is equal to $2/3\pi$, which is the size of each region. $\Delta\eta = 1.6$ corresponds to the acceptance in pseudorapidity. The leading track is not included in the final distributions.

JHEP07(2012)116

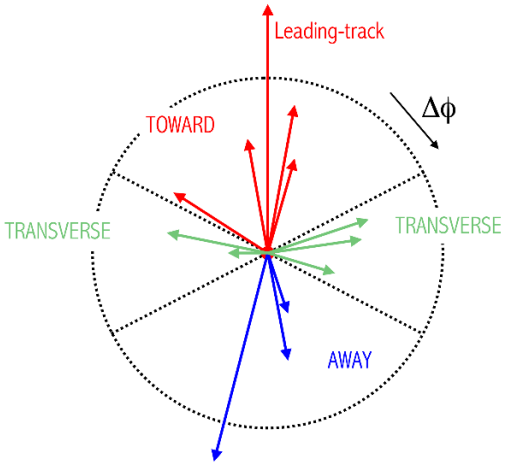

Figure 1. Definition of the regions Toward, Transverse and Away w.r.t. leading track direction.

6 Corrections

We correct for the following detector effects: vertex reconstruction efficiency, tracking efficiency, contamination from secondary particles and leading-track misidentification bias. The various corrections are explained in more detail in the following subsections. We do not correct for the trigger efficiency since its value is basically 100% for events which have at least one particle with $p_{\mathrm{T}} > 0.15\,\mathrm{GeV}/c$ in the range $|\eta| < 0.8$. In table 3 we summarize the maximum effect of each correction on the measured final observables at the two collision energies for $p_{\mathrm{T,min}} = 0.5\,\mathrm{GeV}/c$.

Vertex reconstruction. The correction for finite vertex reconstruction efficiency is performed as a function of the measured multiplicity. Its value is smaller than 0.7% and 0.3% at $\sqrt{s} = 0.9$ and $\sqrt{s} = 7\,\mathrm{TeV}$, respectively.

Tracking efficiency. The tracking efficiency depends on the track level observables η and p_{T}. The projections of the tracking efficiency on the p_{T} and η axes are shown in figure 2. In the pseudorapidity projection we observe a dip of about 1% at $\eta = 0$ due to the central TPC cathode. The slight asymmetry between positive and negative η is due to a different number of active SPD and SDD modules in the two halves of the detector. The number of active modules also differs between the data-taking periods at the two collision energies. Moreover, the efficiency decreases by 5% in the range 1–3 GeV/c. This is due to the fact that above about $1\,\mathrm{GeV}/c$ tracks are almost straight and can be contained completely in the dead areas between TPC sectors. Therefore, at high p_{T} the efficiency is dominated by geometry and has a constant value of about 80% at both collision energies. To avoid statistical fluctuations, the estimated efficiency is fitted with a constant for $p_{\mathrm{T}} > 5\,\mathrm{GeV}/c$ (not shown in the figure).

JHEP07(2012)116

Correction	$\sqrt{s} = 0.9$ TeV	$\sqrt{s} = 7$ TeV
Leading track misidentification	$< 5\%$	$< 8\%$
Contamination	$< 3\%$	$< 3\%$
Efficiency	$< 19\%$	$< 19\%$
Vertex reconstruction	$< 0.7\%$	$< 0.3\%$

Table 3. Maximum effect of corrections on final observables for $p_{\mathrm{T,min}} = 0.5\,\mathrm{GeV}/c$.

Contamination from secondaries. We correct for secondary tracks that pass the track selection cuts. Secondary tracks are predominantly produced by weak decays of strange particles (e.g. K^0_S and Λ), photon conversions or hadronic interactions in the detector material, and decays of charged pions. The relevant track level observables for the contamination correction are transverse momentum and pseudorapidity. The correction is determined from detector simulations and is found to be 15–20% for tracks with $p_{\mathrm{T}} < 0.5\,\mathrm{GeV}/c$ and saturates at about 2% for higher transverse momenta (see figure 3).

We multiply the contamination estimate by a data-driven coefficient to take into account the low strangeness yield in the Monte Carlo compared to data [24]. The coefficient is derived from a fit of the discrepancy between data and Monte Carlo strangeness yields in the tails of the DCA_{XY} distribution which are predominantly populated by secondaries. The factor has a maximum value of 1.07 for tracks with $p_{\mathrm{T}} < 0.5\,\mathrm{GeV}/c$ and is equal to 1 for $p_{\mathrm{T}} > 1.5\,\mathrm{GeV}/c$. This factor is included in the Contamination entry in table 3.

Leading-track misidentification. Experimentally, the real leading track can escape detection because of tracking inefficiency and the detector's finite acceptance. In these cases another track (i.e. the sub-leading or sub-sub-leading etc.) will be selected as the leading one, thus biasing the analysis in two possible ways. Firstly, the sub-leading track will have a different transverse momentum than the leading one. We refer to this as leading-track p_{T} bin migration. It has been verified with Monte Carlo that this effect is negligible due to the weak dependence of the final distributions on $p_{\mathrm{T,LT}}$. Secondly, the reconstructed leading track might have a significantly different orientation with respect to the real one, resulting in a rotation of the overall event topology. The largest bias occurs when the misidentified leading track falls in the Transverse region defined by the real leading track.

We correct for leading-track misidentification with a data-driven procedure. Starting from the measured distributions, for each event the track loss due to inefficiency is applied a second time to the data (having been applied the first time naturally by the detector) by rejecting tracks randomly. If the leading track is considered reconstructed it is used as before to define the different regions. Otherwise the sub-leading track is used. Since the tracking inefficiency is quite small (about 20%) applying it on the reconstructed data a second time does not alter the results significantly. To verify this statement we compared our results with a two step procedure. In this case the inefficiency is applied two times on measured data, half of its value at a time. The correction factor obtained in this way is compatible with the one step procedure. Furthermore, the data-driven procedure has

JHEP07(2012)116

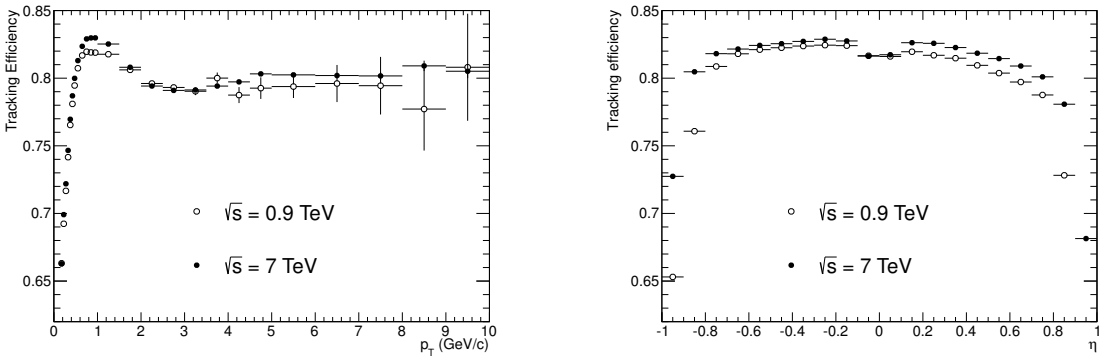

Figure 2. Tracking efficiency vs. track p_{T} (left, $|\eta| < 0.8$) and η (right, $p_{\mathrm{T}} > 0.5\,\mathrm{GeV}/c$) from a Pythia 6.4 and Geant3 simulation.

been tested on simulated data where the true leading particle is known. We observed a discrepancy between the two methods, especially at low leading-track p_{T} values, which is taken into account in the systematic error. The maximum leading-track misidentification correction is 8% on the final distributions.

Two-track effects. By comparing simulated events corrected for single-particle efficiencies with the input Monte Carlo, we observe a 0.5% discrepancy around $\Delta\phi = 0$. This effect is called non-closure in Monte Carlo (it will be discussed further in section 7) and in this case is related to small two-track resolution effects. Data are corrected for this discrepancy.

7 Systematic uncertainties

In tables 4, 5 and 6 we summarize the systematic uncertainties evaluated in the analysis for the three track thresholds: $p_{\mathrm{T}} > 0.15$, 0.5 and $1.0\,\mathrm{GeV}/c$. Each uncertainty is explained in more detail in the following subsections. Uncertainties which are constant as a function of leading-track p_{T} are listed in table 4. Leading-track p_{T} dependent uncertainties are summarized in tables 5 and 6 for $\sqrt{s} = 0.9\,\mathrm{TeV}$ and 7 TeV, respectively. Positive and negative uncertainties are propagated separately, resulting in asymmetric final uncertainties.

Particle composition. The tracking efficiency and contamination corrections depend slightly on the particle species mainly due to their decay length and absorption in the material. To assess the effect of an incorrect description of the particle abundances in the Monte Carlo, we varied the relative yields of pions, protons, kaons, and other particles by 30% relative to the default Monte Carlo predictions. The maximum variation of the final values is 0.9% and represents the systematic uncertainty related to the particle composition (see table 4).

Moreover, we have compared our assessment of the underestimation of strangeness yields with a direct measurement from the ALICE collaboration [24]. Based on the discrepancy between the two estimates, we assign a systematic uncertainty of 0–2.3% depending on the p_{T} threshold and collision energy, see tables 5 and 6.

JHEP07(2012)116

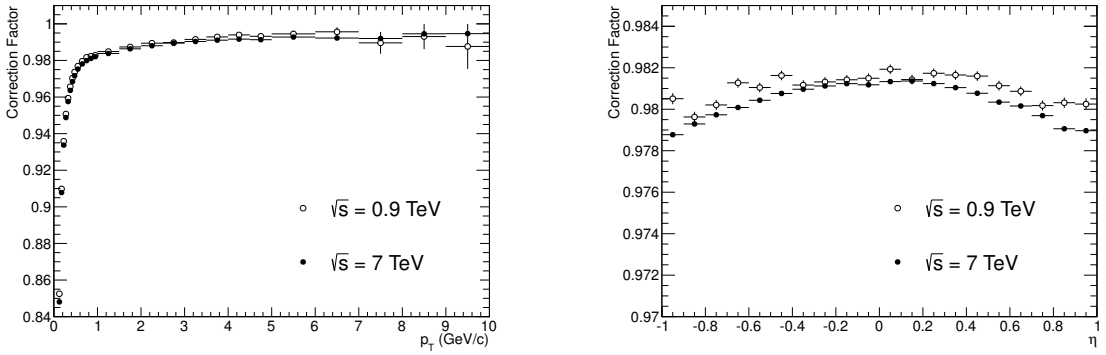

Figure 3. Contamination correction: correction factor vs. track p_{T} (left, $|\eta| < 0.8$) and η (right, $p_{\mathrm{T}} > 0.5\,\mathrm{GeV}/c$) from a PYTHIA 6.4 and GEANT3 simulation.

ITS and TPC efficiency. The tracking efficiency depends on the level of precision of the description of the ITS and TPC detectors in the simulation and the modeling of their response. After detector alignment with survey methods, cosmic-ray events and pp collision events [28], the uncertainty on the efficiency due to the ITS description is estimated to be below 2% and affects only tracks with $p_{\mathrm{T}} < 0.3\,\mathrm{GeV}/c$. The uncertainty due to the TPC reaches 4.5% at very low p_{T} and is smaller than 1.2% for tracks with $p_{\mathrm{T}} > 0.5\,\mathrm{GeV}/c$. The resulting maximum uncertainty on the final distributions is below 1.9%. Moreover, an uncertainty of 1% is included to account for uncertainties in the MC description of the matching between TPC and ITS tracks (see table 4).

Track cuts. By applying the efficiency and contamination corrections we correct for those particles which are lost due to detector effects and for secondary tracks which have not been removed by the selection cuts. These corrections rely on detector simulations and therefore, one needs to estimate the systematic uncertainty introduced in the correction procedure by one particular choice of track cuts. To do so, we repeat the analysis with different values of the track cuts, both for simulated and real data. The variation of the final distributions with different track cuts is a measure of the systematic uncertainty. The overall effect, considering all final distributions, is smaller than 3.5% at both collision energies (see table 4).

Misidentification bias. The uncertainty on the leading-track misidentification correction is estimated from the discrepancy between the data-driven correction used in the analysis and that based on simulations. The effect influences only the first two leading-track p_{T} bins at both collision energies. The maximum uncertainty ($\sim 18\%$) affects the first leading-track p_{T} bin for the track p_{T} cut-off of $0.15\,\mathrm{GeV}/c$. In all other bins this uncertainty is of the order of few percent. As summarized in tables 5 and 6, the uncertainty has slightly different values for the various UE distributions.

Vertex-reconstruction efficiency. The analysis accepts reconstructed vertices with at least one contributing track. We repeat the analysis requiring at least two contributing tracks. The systematic uncertainty related to the vertex reconstruction efficiency is given

JHEP07(2012)116

	$\sqrt{s} = 0.9$ **TeV**		
	$p_{\mathrm{T}} > 0.15\,\mathrm{GeV}/c$	$p_{\mathrm{T}} > 0.5\,\mathrm{GeV}/c$	$p_{\mathrm{T}} > 1.0\,\mathrm{GeV}/c$
Particle composition	± 0.9%	± 0.7%	± 0.4%
ITS efficiency	± 0.6%	—	—
TPC efficiency	± 1.9%	± 0.8%	± 0.4%
Track cuts	$^{+\ 3.0\%}_{-\ 1.1\%}$	$^{+\ 2.0\%}_{-\ 1.1\%}$	$^{+\ 0.9\%}_{-\ 1.5\%}$
ITS/TPC matching	± 1.0%	± 1.0%	± 1.0%
MC dependence	+ 1.1% , + 1.1% , + 1.6%	+ 0.9%	+ 0.9% , + 0.9% , + 1.3%
Material budget	± 0.6%	± 0.2%	± 0.2%
	$\sqrt{s} = 7$ **TeV**		
	$p_{\mathrm{T}} > 0.15\,\mathrm{GeV}/c$	$p_{\mathrm{T}} > 0.5\,\mathrm{GeV}/c$	$p_{\mathrm{T}} > 1.0\,\mathrm{GeV}/c$
Particle composition	± 0.9%	± 0.7%	± 0.5%
ITS efficiency	± 0.5%	—	—
TPC efficiency	± 1.8%	± 0.8%	± 0.5%
Track cuts	$^{+\ 2.1\%}_{-\ 2.3\%}$	$^{+\ 1.6\%}_{-\ 3.2\%}$	$^{+\ 2.5\%}_{-\ 3.5\%}$
ITS/TPC matching	± 1.0%	± 1.0%	± 1.0%
MC dependence	+ 0.8% , + 0.8% , + 1.2%	+ 0.8%	+ 1.0%
Material budget	± 0.6%	± 0.2%	± 0.2%

Table 4. Constant systematic uncertainties at both collision energies. When more than one number is quoted, separated by a comma, the first value refers to the number density distribution, the second to the summed p_{T} and the third to the azimuthal correlation. Some of the uncertainties are quoted asymmetrically.

by the maximum variation in the final distributions between the cases of one and two contributing tracks. Its value is 2.4% for $p_{\mathrm{T,min}} = 0.15\,\mathrm{GeV}/c$ and below 1% for the other cut-off values (see tables 5 and 6). The effect is only visible in the first leading-track p_{T} bin.

Non-closure in Monte Carlo. By correcting a Monte Carlo prediction after full detector simulation with corrections extracted from the same generator, we expect to obtain the input Monte Carlo prediction within the statistical uncertainty. This consideration holds true only if each correction is evaluated with respect to all the variables to which the given correction is sensitive. Any statistically significant difference between input and corrected distributions is referred to as *non-closure in Monte Carlo*.

The overall non-closure effect is sizable ($\sim 17\%$) in the first leading-track p_{T} bin and is 0.6–5.3% in all other bins at both collision energies.

Monte-Carlo dependence. The difference in final distributions when correcting the data with PYTHIA 6.4 or PHOJET generators is of the order of 1% and equally affects all the leading-track p_{T} bins.

Material budget. The material budget has been measured by reconstructing photon conversions which allows a precise γ-ray tomography of the ALICE detector. For the detector regions important for this analysis the remaining uncertainty on the extracted

JHEP07(2012)116

		$\sqrt{s} = 0.9\,\mathbf{TeV}$		
		Number density		
	$p_{\mathrm{T,LT}}$	$p_{\mathrm{T}} > 0.15\,\mathrm{GeV}/c$	$p_{\mathrm{T}} > 0.5\,\mathrm{GeV}/c$	$p_{\mathrm{T}} > 1.0\,\mathrm{GeV}/c$
Lead. track misid.	1^{st} bin	+ (17.8, 16.3, 16.3)%	+ (4.6, 3.5, 3.5)%	+ (4.2, 2.9, 1.7)%
	2^{nd} bin	+ 2.9%	+ 1.3%	—
MC non closure	1^{st} bin	− 17.2%	− 3.6%	− 1.2%
	2^{nd} bin	− 3.2%	− 0.8%	− 1.2%
	others	− 0.6%	− 0.8%	− 1.2%
Strangeness	1^{st} bin	± 1.9%	± 0.2%	—
	others	± 1.0%	± 0.2%	—
Vertex reco.	1^{st} bin	− 2.4%	− 0.7%	− 0.5%
		Summed p_{T}		
	$p_{\mathrm{T,LT}}$	$p_{\mathrm{T}} > 0.15\,\mathrm{GeV}/c$	$p_{\mathrm{T}} > 0.5\,\mathrm{GeV}/c$	$p_{\mathrm{T}} > 1.0\,\mathrm{GeV}/c$
Lead. track misid.	1^{st} bin	+ (20.0, 18.1, 18.1)%	+ (5.3, 4.1, 4.1)%	+ (4.8, 3.4, 3.4)%
	2^{nd} bin	+ 3.7%	+ 1.6%	—
MC non closure	1^{st} bin	− 17.0%	− 2.8%	− 1.1%
	2^{nd} bin	− 3.0%	− 1.0%	− 1.1%
	others	− 0.7%	− 1.0%	− 1.1%
Strangeness	1^{st} bin	± 1.9%	± 0.2%	—
	others	± 1.0%	± 0.2%	—
Vertex reco.	1^{st} bin	− 2.4%	− 0.7%	− 0.5%
		Azimuthal correlation		
	$p_{\mathrm{T,LT}}$	$p_{\mathrm{T}} > 0.15\,\mathrm{GeV}/c$	$p_{\mathrm{T}} > 0.5\,\mathrm{GeV}/c$	$p_{\mathrm{T}} > 1.0\,\mathrm{GeV}/c$
Lead. track misid.	1^{st} bin	+ 12.0%	+ 3.9%	+ 2.5%
	2^{nd} bin	+ 2.6%	+ 1.1%	—
MC non closure	1^{st} bin	− 17.1%	− 3.3%	− 1.6%
	2^{nd} bin	− 3.5%	− 3.0%	− 1.6%
	others	− 2.4%	− 3.0%	− 1.6%
Strangeness	1^{st} bin	± 1.9%	± 0.2%	—
	others	± 1.0%	± 0.2%	—
Vertex reco.	1^{st} bin	− 2.4%	− 0.4%	—
	others	− 0.5%	− 0.4%	—

Table 5. Systematic uncertainties vs. leading track p_{T} at $\sqrt{s} = 0.9\,\mathrm{TeV}$. When more than one number is quoted, separated by a comma, the first value refers to the Toward, the second to the Transverse and the third to the Away region. The second column denotes the leading track p_{T} bin for which the uncertainty applies. The numbering starts for each case from the first bin above the track p_{T} threshold.

material budget is less than 7%. Varying the material density in the detector simulation, the effect on the observables presented is determined to be 0.2–0.6% depending on the p_{T} threshold considered.

JHEP07(2012)116

		$\sqrt{s} = 7$ **TeV**		
		Number density		
	$p_{\mathrm{T,LT}}$	$p_{\mathrm{T}} > 0.15\,\mathrm{GeV}/c$	$p_{\mathrm{T}} > 0.5\,\mathrm{GeV}/c$	$p_{\mathrm{T}} > 1.0\,\mathrm{GeV}/c$
Lead. track misid.	1^{st} bin	+ (17.9, 16.3, 16.3)%	+ (4.0, 3.2, 3.2)%	+ (2.5, 1.2, 1.2)%
	2^{nd} bin	+ 2.7%	—	+ 0.7%
MC non closure	1^{st} bin	− 16.8%	− 2.6%	− 1.9%
	2^{nd} bin	− 2.9%	− 1.4%	− 1.9%
	others	− 0.6%	− 1.0%	− 1.9%
Strangeness	1^{st} bin	± 1.8%	± 2.3%	—
	others	± 1.0%	± 2.3%	—
Vertex reco.	1^{st} bin	− 2.4%	− 0.7%	− 0.5%
		Summed p_{T}		
	$p_{\mathrm{T,LT}}$	$p_{\mathrm{T}} > 0.15\,\mathrm{GeV}/c$	$p_{\mathrm{T}} > 0.5\,\mathrm{GeV}/c$	$p_{\mathrm{T}} > 1.0\,\mathrm{GeV}/c$
Lead. track misid.	1^{st} bin	+ (20.0, 17.9, 17.9)%	+ (4.9, 3.8, 3.8)%	+ (3.4, 1.9, 1.9)%
	2^{nd} bin	+ 3.4%	+ 0.8%	+ 1.1%
MC non closure	1^{st} bin	− 16.7%	− 2.7%	− 1.5%
	2^{nd} bin	− 2.6%	− 1.2%	− 1.5%
	others	− 0.8%	− 1.0%	− 1.5%
Strangeness	1^{st} bin	± 1.8%	± 2.3%	—
	others	± 1.0%	± 2.3%	—
Vertex reco.	1^{st} bin	− 2.4%	− 0.7%	− 0.5%
		Azimuthal correlation		
	$p_{\mathrm{T,LT}}$	$p_{\mathrm{T}} > 0.15\,\mathrm{GeV}/c$	$p_{\mathrm{T}} > 0.5\,\mathrm{GeV}/c$	$p_{\mathrm{T}} > 1.0\,\mathrm{GeV}/c$
Lead. track misid.	1^{st} bin	+ 16.8%	+ 3.4%	+ 0.9%
	2^{nd} bin	+ 2.5%	—	—
MC non closure	1^{st} bin	− 25.3%	− 4.3%	− 1.2%
	2^{nd} bin	− 5.3%	− 2.1%	− 1.2%
	others	− 2.1%	− 2.1%	− 1.2%
Strangeness	1^{st} bin	± 1.8%	± 2.3%	—
	others	± 1.0%	± 2.3%	—
Vertex reco.	1^{st} bin	− 2.4%	− 0.4%	—
	others	− 0.5%	− 0.4%	—

Table 6. Systematic uncertainties vs. leading track p_{T} at $\sqrt{s} = 7\,\mathrm{TeV}$. When more than one number is quoted, separated by a comma, the first value refers to the Toward, the second to the Transverse and the third to the Away region. The second column denotes the leading track p_{T} bin for which the uncertainty applies. The numbering starts for each case from the first bin above the track p_{T} threshold.

JHEP07(2012)116

	$\sqrt{s} = 0.9$ **TeV**			
	Number density		**Summed** p_{T}	
	Slope $(\mathrm{GeV}/c)^{-1}$	**Mean**	**Slope**	**Mean** (GeV/c)
$p_{\mathrm{T}} > 0.15\,\mathrm{GeV/c}$	0.00 ± 0.02	1.00 ± 0.04	0.00 ± 0.01	0.62 ± 0.02
$p_{\mathrm{T}} > 0.5\,\mathrm{GeV/c}$	0.00 ± 0.01	0.45 ± 0.02	0.01 ± 0.01	0.45 ± 0.02
$p_{\mathrm{T}} > 1.0\,\mathrm{GeV/c}$	0.003 ± 0.003	0.16 ± 0.01	0.006 ± 0.005	0.24 ± 0.01
	$\sqrt{s} = 7$ **TeV**			
	Number density		**Summed** p_{T}	
	Slope $(\mathrm{GeV}/c)^{-1}$	**Mean**	**Slope**	**Mean** (GeV/c)
$p_{\mathrm{T}} > 0.15\,\mathrm{GeV/c}$	0.00 ± 0.01	1.82 ± 0.06	0.01 ± 0.01	1.43 ± 0.05
$p_{\mathrm{T}} > 0.5\,\mathrm{GeV/c}$	0.005 ± 0.007	0.95 ± 0.03	0.01 ± 0.01	1.15 ± 0.04
$p_{\mathrm{T}} > 1.0\,\mathrm{GeV/c}$	0.001 ± 0.003	0.41 ± 0.01	0.008 ± 0.006	0.76 ± 0.03
	$\sqrt{s} = 1.8$ **TeV (CDF)**			
	Number density (at leading charged jet $p_{\mathrm{T}} = 20\,\mathrm{GeV}/c$**)**			
$p_{\mathrm{T}} > 0.5\,\mathrm{GeV/c}$	0.60			

Table 7. Saturation values in the Transverse region for the two collision energies. The result from CDF is also given, for details see text.

8 Results

In this section we present and discuss the corrected results for the three UE distributions in all regions at the two collision energies. The upper part of each plot shows the relevant measured distribution (black points) compared to a set of Monte Carlo predictions (coloured curves). Shaded bands represent the systematic uncertainty only. Error bars along the x axis indicate the bin width. The lower part shows the ratio between Monte Carlo and data. In this case the shaded band is the sum in quadrature of statistical and systematic uncertainties.

The overall agreement of data and simulations is of the order of 10–30% and we were not able to identify a preferred model that can reproduce all measured observables. In general, all three generators underestimate the event activity in the Transverse region. Nevertheless, an agreement of the order of 20% has to be considered a success, considering the complexity of the system under study. Even though an exhaustive comparison of data with the latest models available is beyond the scope of this paper, in the next sections we will indicate some general trends observed in the comparison with the chosen models.

In the following discussion we define the leading track p_{T} range from 4 to 10 GeV/c at $\sqrt{s} = 0.9\,\mathrm{TeV}$ and from 10 to 25 GeV/c at $\sqrt{s} = 7\,\mathrm{TeV}$ as the *plateau*.

8.1 Number density

In figure 4–6 we show the multiplicity density as a function of leading track p_{T} in the three regions: Toward, Transverse and Away. Toward and Away regions are expected to collect

JHEP07(2012)116

the fragmentation products of the two back-to-back outgoing partons from the elementary hard scattering. We observe that the multiplicity density in these regions increases monotonically with the $p_{\mathrm{T,LT}}$ scale. In the Transverse region, after a monotonic increase at low leading track p_{T}, the distribution tends to flatten out. The same behaviour is observed at both collision energies and all values of $p_{\mathrm{T,min}}$.

The rise with $p_{\mathrm{T,LT}}$ has been interpreted as evidence for an impact parameter dependence in the hadronic collision [29]. More central collisions have an increased probability for MPI, leading to a larger transverse multiplicity. Nevertheless, we must be aware of a trivial effect also contributing to the low $p_{\mathrm{T,LT}}$ region. For instance for any probability distribution, the maximum value per randomized sample averaged over many samples rises steadily with the sample size M. In our case, the conditional probability density $\mathcal{P}(p_{\mathrm{T,LT}}|M)$ shifts towards larger $p_{\mathrm{T,LT}}$ with increasing M. Using Bayes' theorem one expects the conditional probability density $\mathcal{P}(M|p_{\mathrm{T,LT}})$ to shift towards larger M with rising $p_{\mathrm{T,LT}}$:

$$\mathcal{P}(M|p_{\mathrm{T,LT}}) \sim \mathcal{P}(p_{\mathrm{T,LT}}|M)\mathcal{P}(M). \tag{8.1}$$

The saturation of the distribution at higher values of $p_{\mathrm{T,LT}}$ indicates the onset of the event-by-event partitioning into azimuthal regions containing the particles from the hard scattering and the UE region. The bulk particle production becomes independent of the hard scale.

The plateau range is fitted with a line. The fit slopes, consistent with zero, and mean values for the three p_{T} thresholds are reported in table 7. In the fit, potential correlations of the systematic uncertainties in different p_{T} bins are neglected.

ATLAS has published a UE measurement where the hard scale is given by the leading track p_{T}, with a p_{T} threshold for particles of $0.5\,\mathrm{GeV}/c$ and an acceptance of $|\eta| < 2.5$ [7]. Given the different acceptance with respect to our measurement, the results in the Toward and Away regions are not comparable. On the other hand the mean values of the Transverse plateaus from the two measurements are in good agreement, indicating an independence of the UE activity on the pseudorapidity range. The CDF collaboration measured the UE as a function of charged particle jet p_{T} at a collision energy of 1.8 TeV [2]. The particle p_{T} threshold is $0.5\,\mathrm{GeV}/c$ and the acceptance $|\eta| < 1$. In the Transverse region CDF measures 3.8 charged particles per unit pseudorapidity above the p_{T} threshold at leading-jet $p_{\mathrm{T}} = 20\,\mathrm{GeV}/c$. This number needs to be divided by 2π in order to be compared with the average number of particles in the plateau from table 7 at the same threshold value. The scaled CDF result is 0.60, also shown in table 7 for comparison. As expected it falls between our two measurements at $\sqrt{s} = 0.9\,\mathrm{TeV}$ and $\sqrt{s} = 7\,\mathrm{TeV}$. The values do not scale linearly with the collision energy, in particular the increase is higher from 0.9 to 1.8 TeV than from 1.8 to 7 TeV. Interpolating between our measurements assuming a logarithmic dependence on $\sqrt{s}$ results in 0.62 charged particles per unit area at 1.8 TeV, consistent with the CDF result.

For illustration, figure 7 presents the number density in the plateau of the Transverse region for $p_{\mathrm{T}} > 0.5\,\mathrm{GeV}/c$ (our measurement as well as the value measured by CDF at 1.8 TeV) compared with $dN_{\mathrm{ch}}/d\eta|_{\eta=0}$ of charged particles with $p_{\mathrm{T}} > 0.5\,\mathrm{GeV}/c$ in minimum-bias events [32] (scaled by $1/2\pi$).[2] The UE activity in the plateau region is more

[2]These data are for events that have at least one charged particle in $|\eta| < 2.5$.

JHEP07(2012)116

	Number density	**Summed p_{T}**
$p_{\mathrm{T}} > 0.15\,\mathrm{GeV}/c$	1.76 ± 0.02	2.00 ± 0.03
$p_{\mathrm{T}} > 0.5\,\mathrm{GeV}/c$	1.97 ± 0.03	2.16 ± 0.03
$p_{\mathrm{T}} > 1.0\,\mathrm{GeV}/c$	2.32 ± 0.04	2.48 ± 0.05

Table 8. Constant fit in $4 < p_{\mathrm{T,LT}} < 10\,\mathrm{GeV}/c$ to the ratio between $\sqrt{s} = 0.9\,\mathrm{TeV}$ and $\sqrt{s} = 7\,\mathrm{TeV}$ for number density (left) and summed p_{T} (right) distributions in the Transverse region. The shown uncertainties are based on statistical and systematic uncertainties summed in quadrature.

than a factor 2 larger than the $dN_{\mathrm{ch}}/d\eta$. Both can be fitted with a logarithmic dependence on s $(a + b \ln s)$. The relative increase from 0.9 to 7 TeV for the UE is larger than that for the $dN_{\mathrm{ch}}/d\eta$: about 110% compared to about 80%, respectively.

In figure 8 (left) we show the ratio between the number density distribution at $\sqrt{s} = 7\,\mathrm{TeV}$ and $\sqrt{s} = 0.9\,\mathrm{TeV}$. Most of the systematic uncertainties are expected to be correlated between the two energies, therefore we consider only statistical uncertainties. The ratio saturates for leading track $p_{\mathrm{T}} > 4\,\mathrm{GeV}/c$. The results of a constant fit in the range $4 < p_{\mathrm{T,LT}} < 10\,\mathrm{GeV}/c$ are reported in table 8. The measured scaling factor for a p_{T} threshold of $0.5\,\mathrm{GeV}/c$ is in agreement with the observations of ATLAS [7, 30] and CMS [31].

For the track threshold $p_{\mathrm{T}} > 0.15\,\mathrm{GeV}/c$ all models underestimate the charged multiplicity in the Transverse and Away regions. In particular at $\sqrt{s} = 7\,\mathrm{TeV}$ PHOJET predictions largely underestimate the measurement in the Transverse region (up to $\sim 50\%$), the discrepancy being more pronounced with increasing p_{T} cut-off value. Pythia 8 correctly describes the Toward region at both collision energies and Phojet only at $\sqrt{s} = 0.9\,\mathrm{TeV}$. For track $p_{\mathrm{T}} > 1\,\mathrm{GeV}/c$, Pythia 8 systematically overestimates the event activity in the jet fragmentation regions (Toward and Away).

8.2 Summed p_{T}

In figure 9–11 we show the summed p_{T} density as a function of leading track p_{T} in the three topological regions. The shape of the distributions follows a trend similar to that discussed above for the number density.

The general trend of Pythia 8 is to overestimate the fragmentation in the Toward region at all p_{T} cut-off values. Also in this case at $\sqrt{s} = 7\,\mathrm{TeV}$ PHOJET largely underestimates the measurement in the Transverse region (up to $\sim 50\%$), especially at higher values of p_{T} cut-off. Other systematic trends are not very pronounced.

In table 7 we report the mean value of a linear fit in the plateau range. Our results agree with the ATLAS measurement in the Transverse plateau.

In figure 8 (right) we show the ratio between the distribution at $\sqrt{s} = 7\,\mathrm{TeV}$ and $\sqrt{s} = 0.9\,\mathrm{TeV}$, considering as before only statistical errors. The results of a constant fit in the range $4 < p_{\mathrm{T,LT}} < 10\,\mathrm{GeV}/c$ are reported in table 8. Also in this case the scaling factor is in agreement with ATLAS and CMS results.

The summed p_{T} density in the Transverse region can be interpreted as a measurement of the UE activity in a given leading track p_{T} bin. Therefore, its value in the plateau can be used, for example, to correct jet spectra.

JHEP07(2012)116

8.3 Azimuthal correlation

In figure 12–22 azimuthal correlations between tracks and the leading track are shown in different ranges of leading track p_{T}. The range $1/3\pi < |\Delta\phi| < 2/3\pi$ corresponds to the Transverse region. The regions $-1/3\pi < \Delta\phi < 1/3\pi$ (Toward) and $2/3\pi < |\Delta\phi| < \pi$ (Away) collect the fragmentation products of the leading and sub-leading jets. In general, all Monte Carlo simulations considered fail to reproduce the shape of the measured distributions. Pythia 8 provides the best prediction for the Transverse activity in all leading track p_{T} ranges considered. Unfortunately the same model significantly overestimates the jet fragmentation regions.

9 Conclusions

We have characterized the Underlying Event in pp collisions at $\sqrt{s} = 0.9$ and 7 TeV by measuring the number density, the summed p_{T} distribution and the azimuthal correlation of charged particles with respect to the leading particle. The analysis is based on about $6 \cdot 10^6$ minimum bias events at $\sqrt{s} = 0.9$ TeV and $25 \cdot 10^6$ events at $\sqrt{s} = 7$ TeV collected during the data taking periods from April to July 2010. Measured data have been corrected for detector related effects; in particular we applied a data-driven correction to account for the misidentification of the leading track. The fully corrected final distributions are compared with Pythia 6.4, Pythia 8 and Phojet, showing that pre-LHC tunes have difficulties describing the data. These results are an important ingredient in the required retuning of those generators.

Among the presented distributions, the Transverse region is particularly sensitive to the Underlying Event. We find that the ratio between the distributions at $\sqrt{s} = 0.9$ and 7 TeV in this region saturates at a value of about 2 for track $p_{\mathrm{T}} > 0.5\,\mathrm{GeV}/c$. The summed p_{T} distribution rises slightly faster as a function of $\sqrt{s}$ than the number density distribution, indicating that the available energy tends to increase the particle's transverse momentum in addition to the multiplicity. This is in qualitative agreement with an increased relative contribution of hard processes to the Underlying Event with increasing $\sqrt{s}$. Moreover, the average number of particles at large $p_{\mathrm{T,LT}}$ in the Transverse region seems to scale logarithmically with the collision energy. In general our results are in good qualitative and quantitative agreement with measurements from other LHC experiments (ATLAS and CMS) and show similar trends to that of the Tevatron (CDF).

Our results show that the activity in the Transverse region increases logarithmically and faster than $dN_{\mathrm{ch}}/d\eta$ in minimum-bias events. Models aiming to correctly reproduce these minimum-bias and underlying event distributions need a precise description of the interplay of the hard process, the associated initial and final-state radiation and multiple parton interactions.

JHEP07(2012)116

Number density — track $p_{\mathrm{T}} > 0.15\,\mathrm{GeV}/c$.

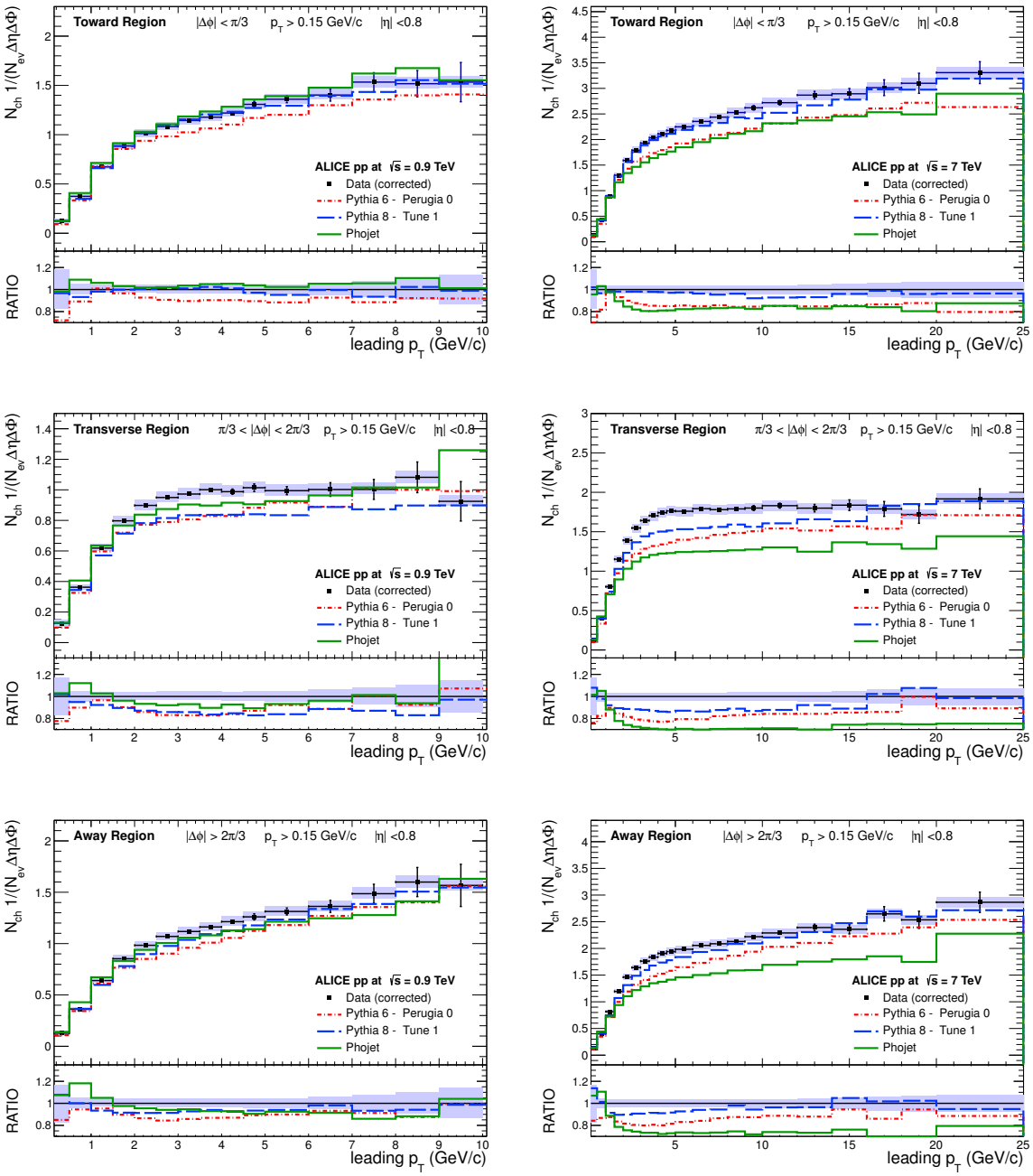

Figure 4. Number density in Toward (top), Transverse (middle) and Away (bottom) regions at $\sqrt{s} = 0.9\,\mathrm{TeV}$ (left) and $\sqrt{s} = 7\,\mathrm{TeV}$ (right). Right and left vertical scales differ by a factor 2. Shaded area in upper plots: systematic uncertainties. Shaded areas in bottom plots: sum in quadrature of statistical and systematic uncertainties. Horizontal error bars: bin width.

JHEP07(2012)116

Number density — track $p_{\mathrm{T}} > 0.5\,\mathrm{GeV}/c$.

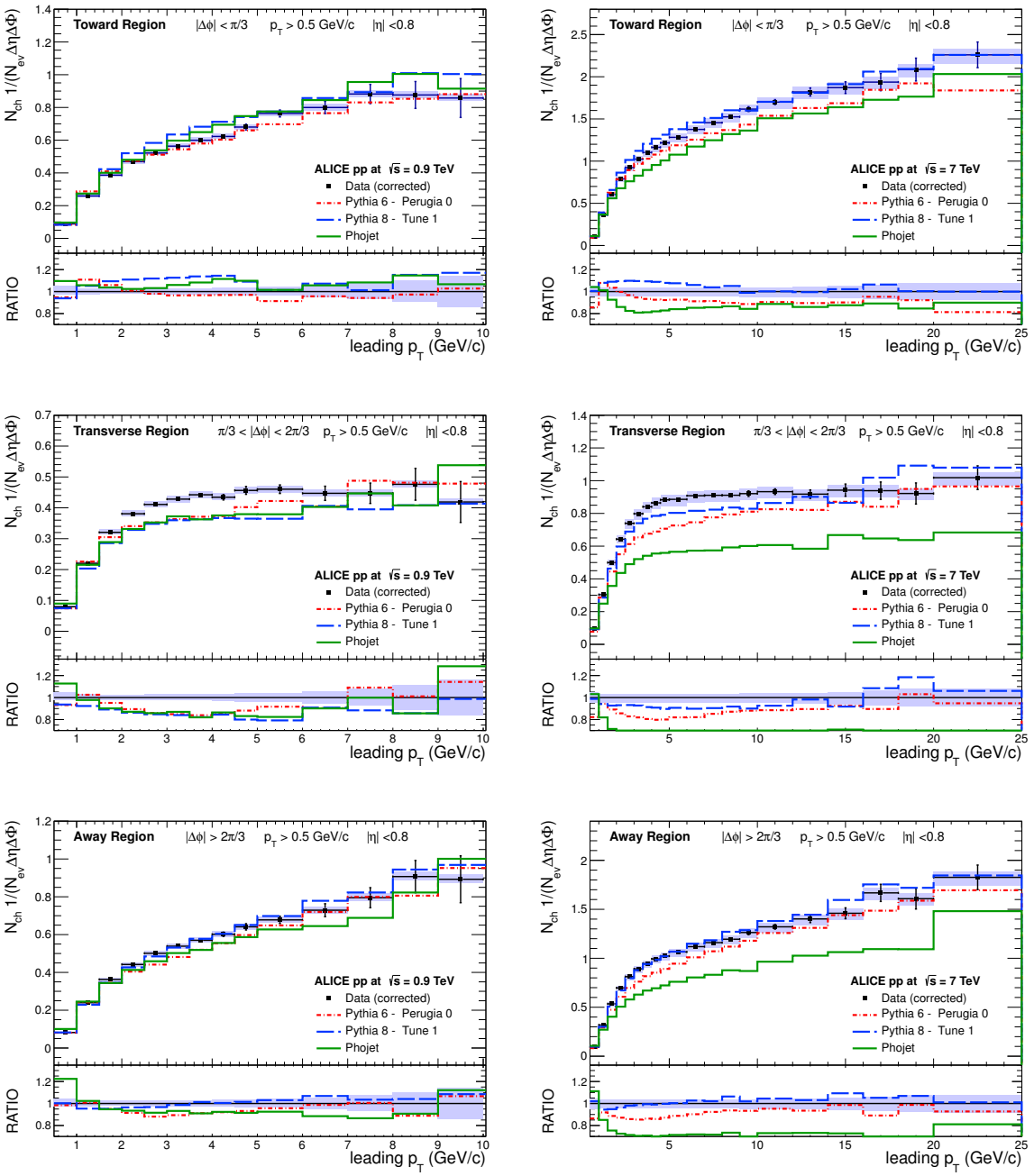

Figure 5. Number density in Toward (top), Transverse (middle) and Away (bottom) regions at $\sqrt{s} = 0.9\,\mathrm{TeV}$ (left) and $\sqrt{s} = 7\,\mathrm{TeV}$ (right). Right and left vertical scales differ by a factor 2. Shaded area in upper plots: systematic uncertainties. Shaded areas in bottom plots: sum in quadrature of statistical and systematic uncertainties. Horizontal error bars: bin width.

JHEP07(2012)116

Number density — track $p_{\mathrm{T}} > 1.0\,\mathrm{GeV}/c$.

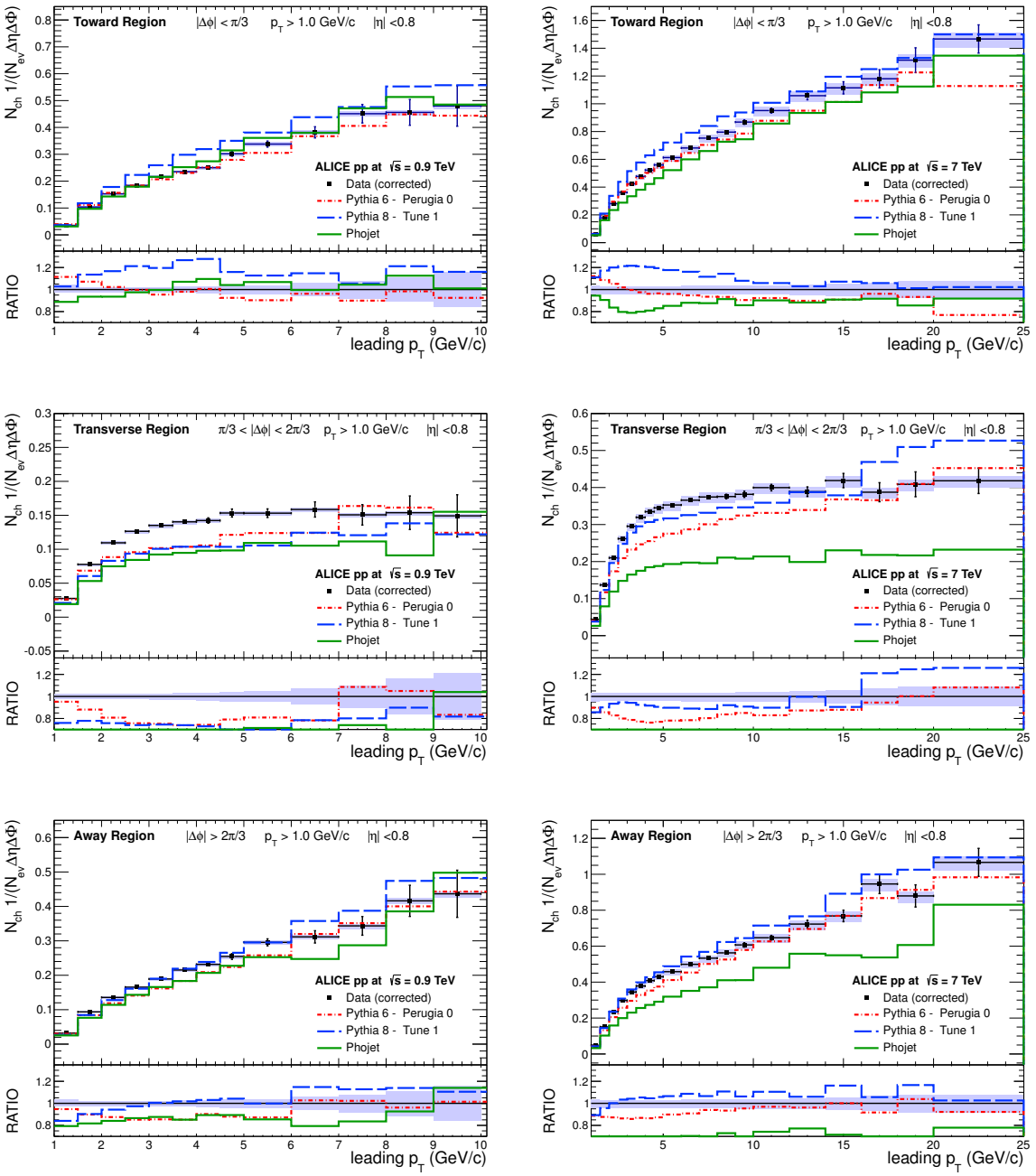

Figure 6. Number density in Toward (top), Transverse (middle) and Away (bottom) regions at $\sqrt{s} = 0.9\,\mathrm{TeV}$ (left) and $\sqrt{s} = 7\,\mathrm{TeV}$ (right). Right and left vertical scales differ by a factor 2. Shaded area in upper plots: systematic uncertainties. Shaded areas in bottom plots: sum in quadrature of statistical and systematic uncertainties. Horizontal error bars: bin width.

JHEP07(2012)116

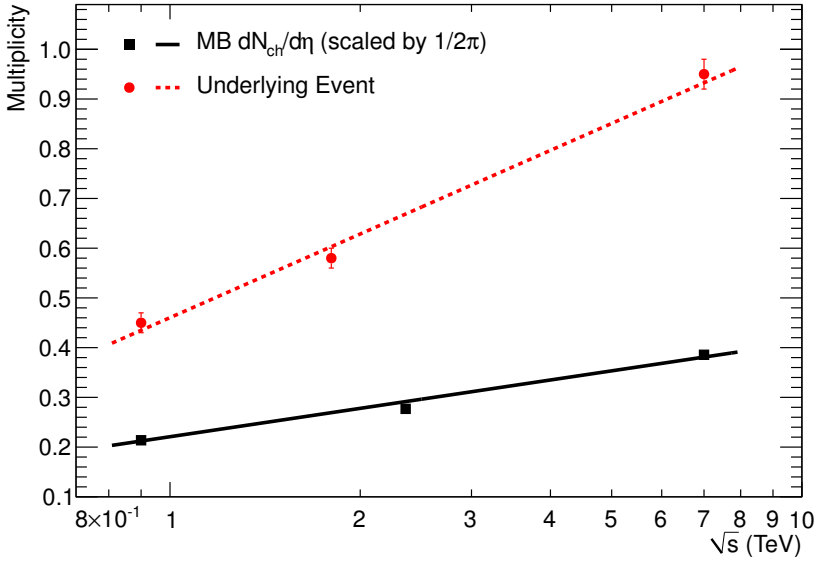

Figure 7. Comparison of number density in the plateau of the Transverse region (see table 8) and $dN_{\rm ch}/d\eta$ in minimum-bias events (scaled by $1/2\pi$) [32]. Both are for charged particles with $p_{\rm T} > 0.5\,{\rm GeV}/c$. For this plot, statistical and systematic uncertainties have been summed in quadrature. The lines show fits with the functional form $a + b \ln s$.

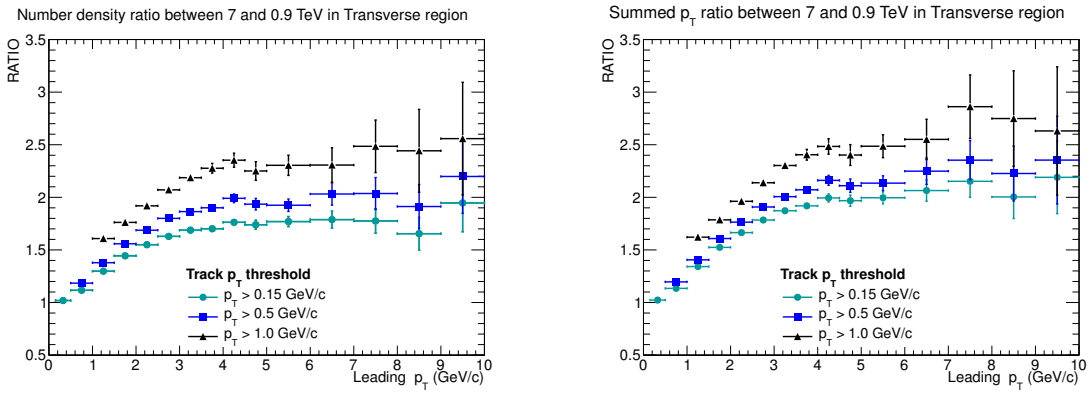

Figure 8. Ratio between $\sqrt{s} = 0.9\,{\rm TeV}$ and $\sqrt{s} = 7\,{\rm TeV}$ for number density (left) and summed $p_{\rm T}$ (right) distributions in the Transverse region. Statistical uncertainties only.

JHEP07(2012)116

Summed p_{T} — track $p_{\mathrm{T}} > 0.15\,\mathrm{GeV}/c$.

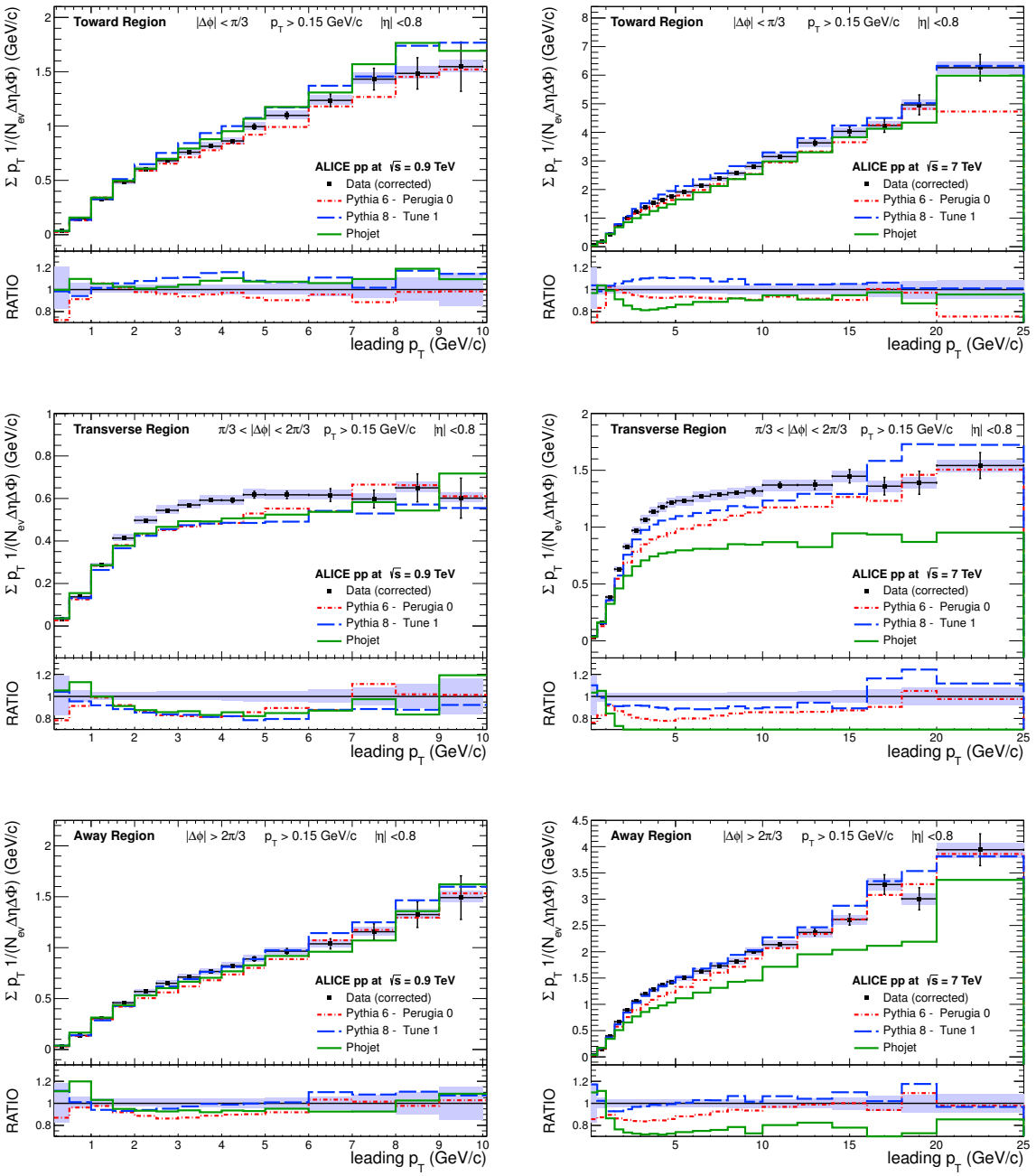

Figure 9. Summed p_{T} in Toward (top), Transverse (middle) and Away (bottom) regions at $\sqrt{s} = 0.9\,\mathrm{TeV}$ (left) and $\sqrt{s} = 7\,\mathrm{TeV}$ (right). Right and left vertical scales differ by a factor 4 (2) in the top (middle and bottom) panel. Shaded area in upper plots: systematic uncertainties. Shaded areas in bottom plots: sum in quadrature of statistical and systematic uncertainties. Horizontal error bars: bin width.

JHEP07(2012)116

Summed p_{T} — track $p_{\mathrm{T}} > 0.5\,\mathrm{GeV}/c$.

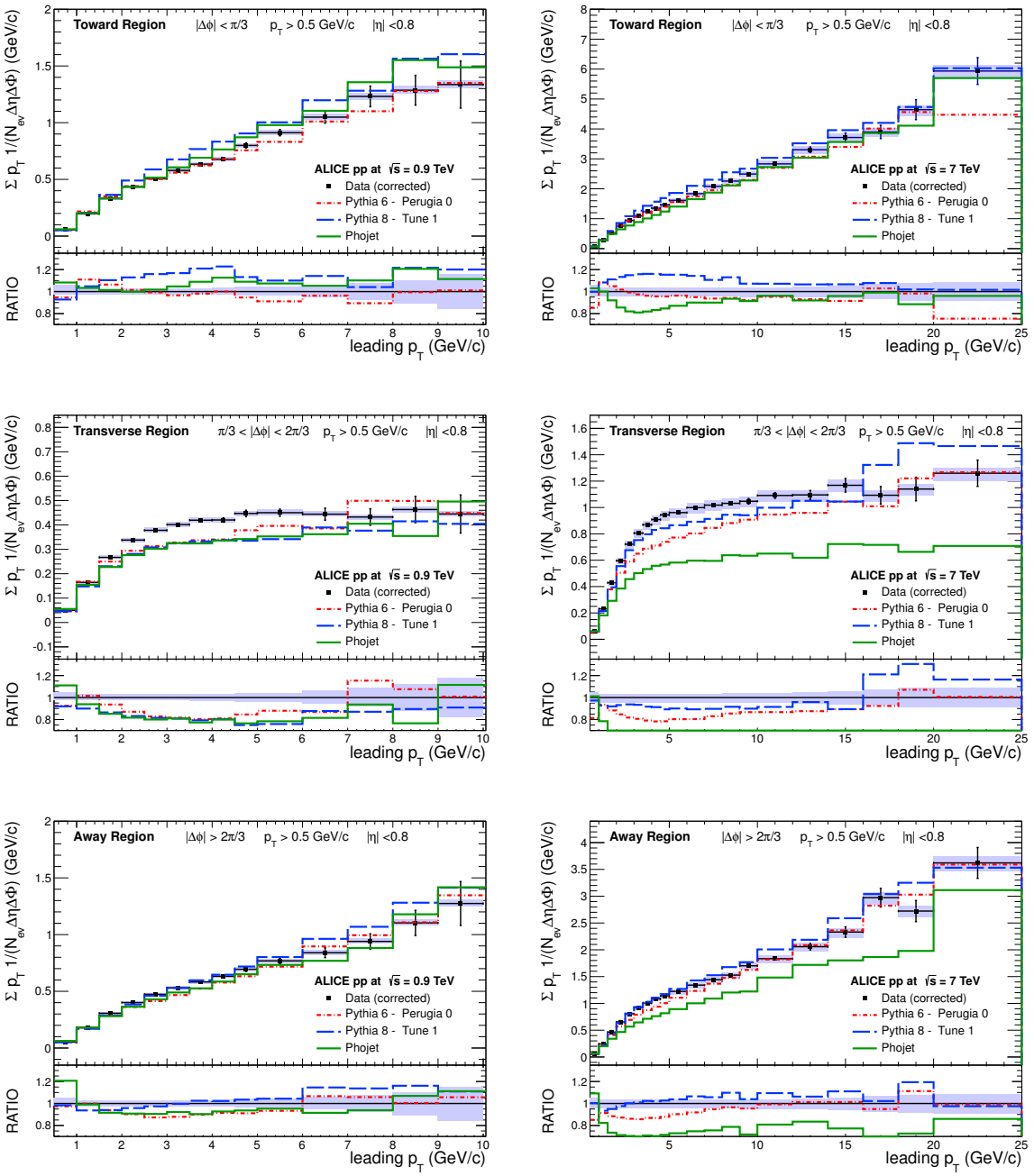

Figure 10. Summed p_{T} in Toward (top), Transverse (middle) and Away (bottom) regions at $\sqrt{s} = 0.9\,\mathrm{TeV}$ (left) and $\sqrt{s} = 7\,\mathrm{TeV}$ (right). Right and left vertical scales differ by a factor 4 (2) in the top (middle and bottom) panel. Shaded area in upper plots: systematic uncertainties. Shaded areas in bottom plots: sum in quadrature of statistical and systematic uncertainties. Horizontal error bars: bin width.

JHEP07(2012)116

Summed p_{T} — track $p_{\mathrm{T}} > 1.0\,\mathrm{GeV}/c$.

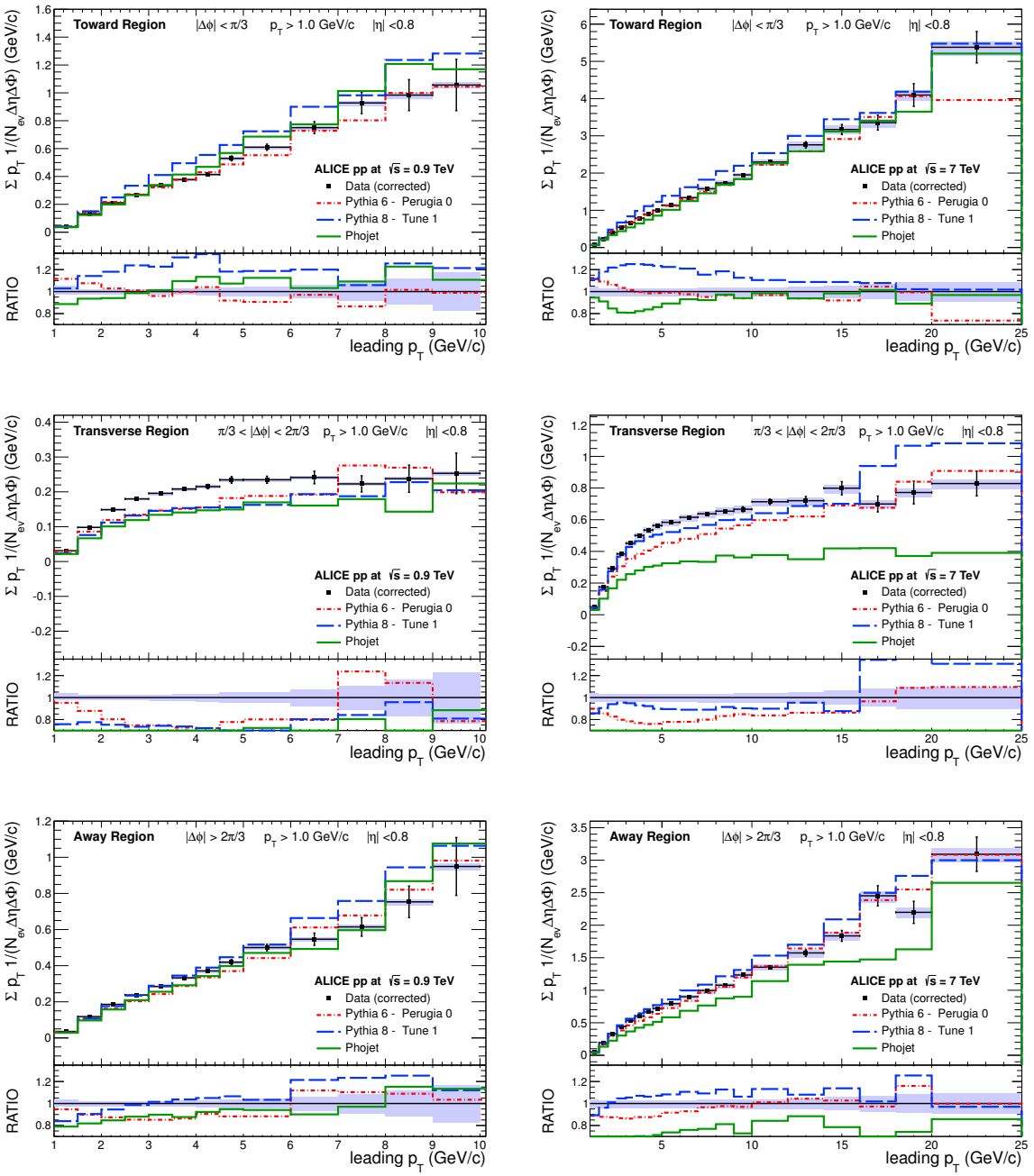

Figure 11. Summed p_{T} in Toward (top), Transverse (middle) and Away (bottom) regions at $\sqrt{s} = 0.9\,\mathrm{TeV}$ (left) and $\sqrt{s} = 7\,\mathrm{TeV}$ (right). Right and left vertical scales differ by a factor 4 (3) in the top (middle and bottom) panel. Shaded area in upper plots: systematic uncertainties. Shaded areas in bottom plots: sum in quadrature of statistical and systematic uncertainties. Horizontal error bars: bin width.

JHEP07(2012)116

Azimuthal correlations — track $p_{\mathrm{T}} > 0.15\,\mathrm{GeV}/c$.

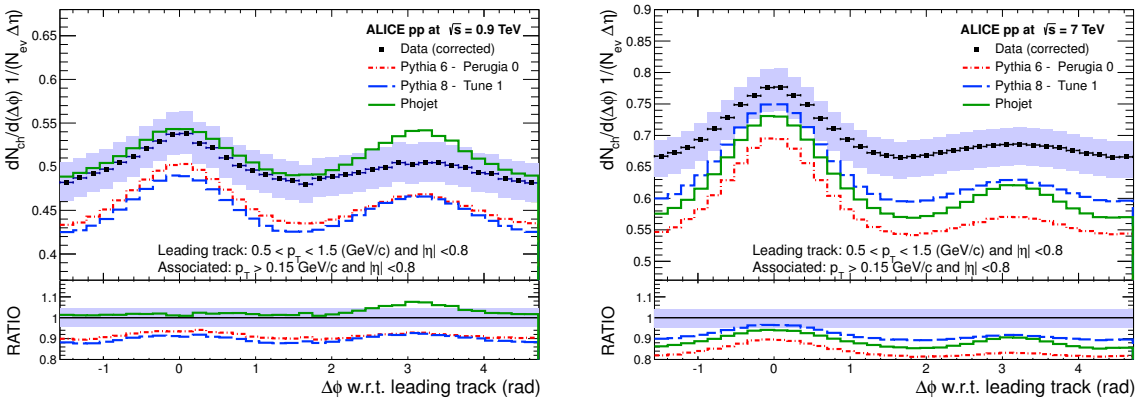

Figure 12. Azimuthal correlation at $\sqrt{s} = 0.9\,\mathrm{TeV}$ (left) and $\sqrt{s} = 7\,\mathrm{TeV}$ (right). Leading-track: $0.5 < p_{T,LT} < 1.5\,\mathrm{GeV}/c$. For visualization purposes the $\Delta\phi$ axis is not centered around 0. Shaded area in upper plots: systematic uncertainties. Shaded areas in bottom plots: sum in quadrature of statistical and systematic uncertainties. Horizontal error bars: bin width.

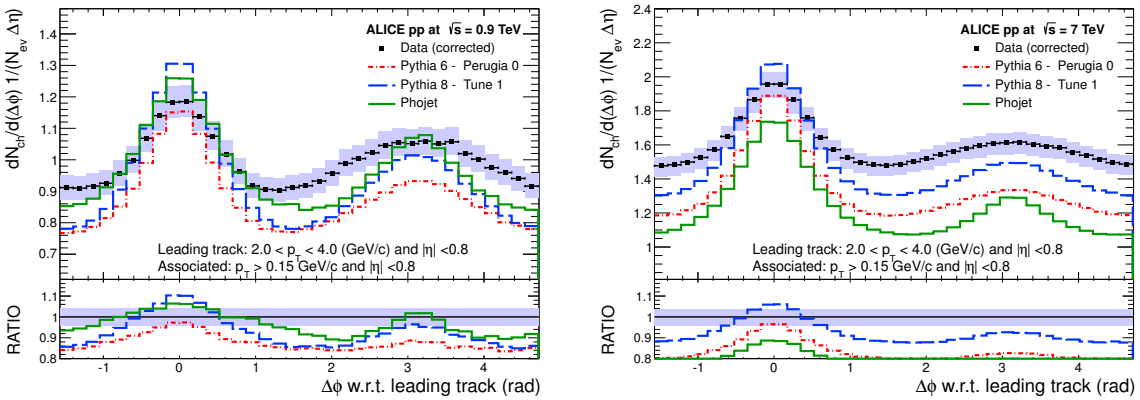

Figure 13. Azimuthal correlation at $\sqrt{s} = 0.9\,\mathrm{TeV}$ (left) and $\sqrt{s} = 7\,\mathrm{TeV}$ (right). Leading-track: $2.0 < p_{T,LT} < 4.0\,\mathrm{GeV}/c$. For visualization purposes the $\Delta\phi$ axis is not centered around 0. Shaded area in upper plots: systematic uncertainties. Shaded areas in bottom plots: sum in quadrature of statistical and systematic uncertainties. Horizontal error bars: bin width.

JHEP07(2012)116

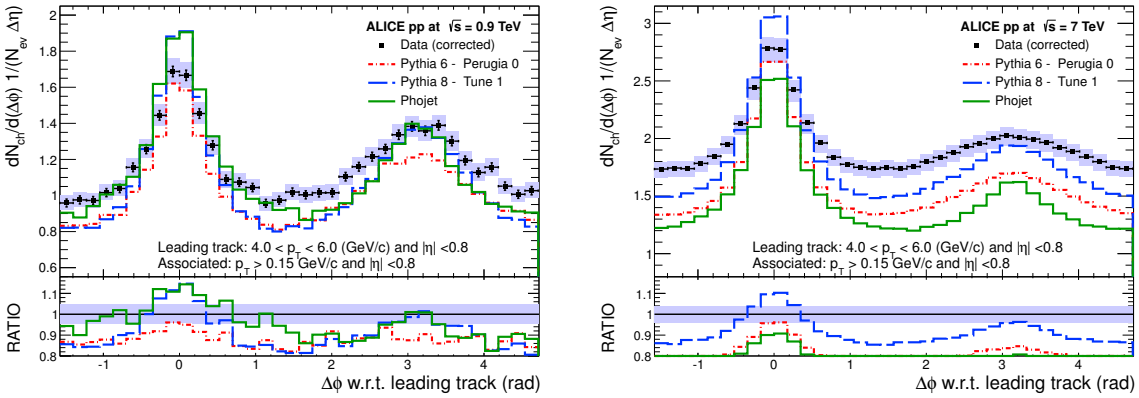

Figure 14. Azimuthal correlation at $\sqrt{s} = 0.9\,\text{TeV}$ (left) and $\sqrt{s} = 7\,\text{TeV}$ (right). Leading-track: $4.0 < p_{T,LT} < 6.0\,\text{GeV}/c$. For visualization purposes the $\Delta\phi$ axis is not centered around 0. Shaded area in upper plots: systematic uncertainties. Shaded areas in bottom plots: sum in quadrature of statistical and systematic uncertainties. Horizontal error bars: bin width.

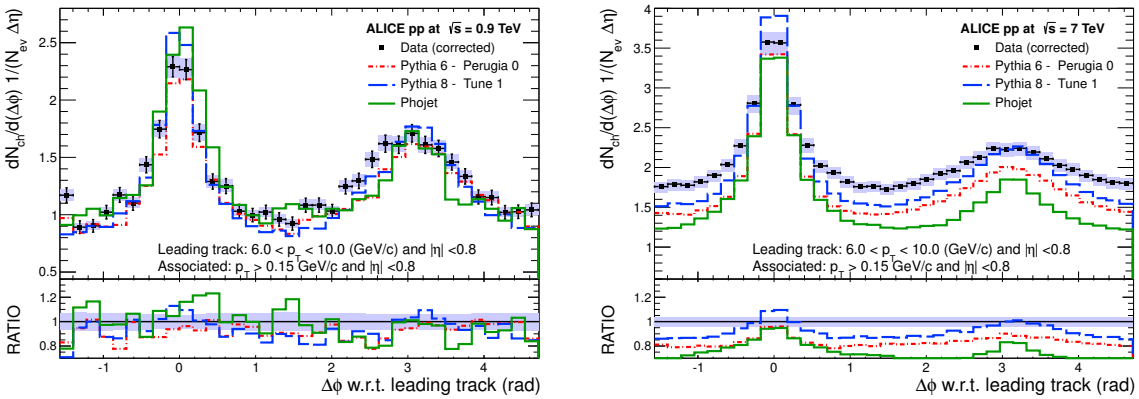

Figure 15. Azimuthal correlation at $\sqrt{s} = 0.9\,\text{TeV}$ (left) and $\sqrt{s} = 7\,\text{TeV}$ (right). Leading-track: $6.0 < p_{T,LT} < 10.0\,\text{GeV}/c$. For visualization purposes the $\Delta\phi$ axis is not centered around 0. Shaded area in upper plots: systematic uncertainties. Shaded areas in bottom plots: sum in quadrature of statistical and systematic uncertainties. Horizontal error bars: bin width.

JHEP07(2012)116

Azimuthal correlations — track $p_{\mathrm{T}} > 0.5\,\mathrm{GeV}/c$.

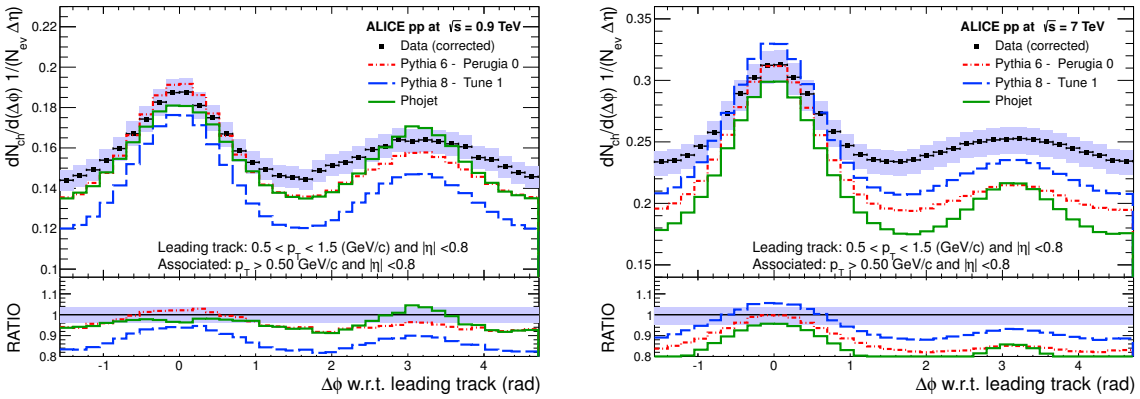

Figure 16. Azimuthal correlation at $\sqrt{s} = 0.9\,\mathrm{TeV}$ (left) and $\sqrt{s} = 7\,\mathrm{TeV}$ (right). Leading-track: $0.5 < p_{T,LT} < 1.5\,\mathrm{GeV}/c$. For visualization purposes the $\Delta\phi$ axis is not centered around 0. Shaded area in upper plots: systematic uncertainties. Shaded areas in bottom plots: sum in quadrature of statistical and systematic uncertainties. Horizontal error bars: bin width.

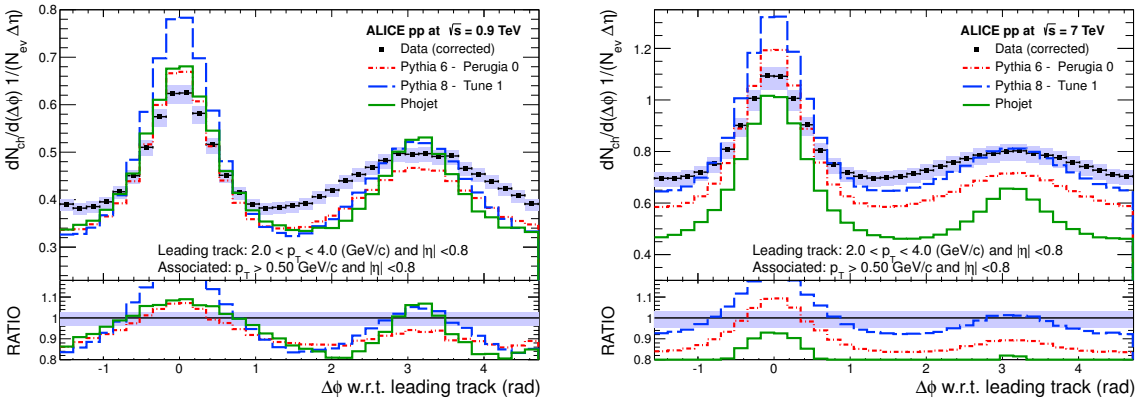

Figure 17. Azimuthal correlation at $\sqrt{s} = 0.9\,\mathrm{TeV}$ (left) and $\sqrt{s} = 7\,\mathrm{TeV}$ (right). Leading-track: $2.0 < p_{T,LT} < 4.0\,\mathrm{GeV}/c$. For visualization purposes the $\Delta\phi$ axis is not centered around 0. Shaded area in upper plots: systematic uncertainties. Shaded areas in bottom plots: sum in quadrature of statistical and systematic uncertainties. Horizontal error bars: bin width.

JHEP07(2012)116

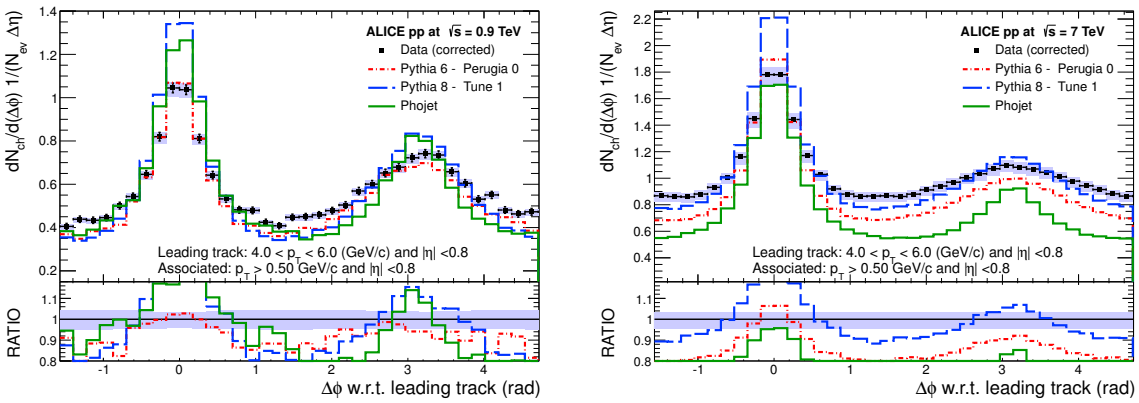

Figure 18. Azimuthal correlation at $\sqrt{s} = 0.9\,\text{TeV}$ (left) and $\sqrt{s} = 7\,\text{TeV}$ (right). Leading-track: $4.0 < p_{T,LT} < 6.0\,\text{GeV}/c$. For visualization purposes the $\Delta\phi$ axis is not centered around 0. Shaded area in upper plots: systematic uncertainties. Shaded areas in bottom plots: sum in quadrature of statistical and systematic uncertainties. Horizontal error bars: bin width.

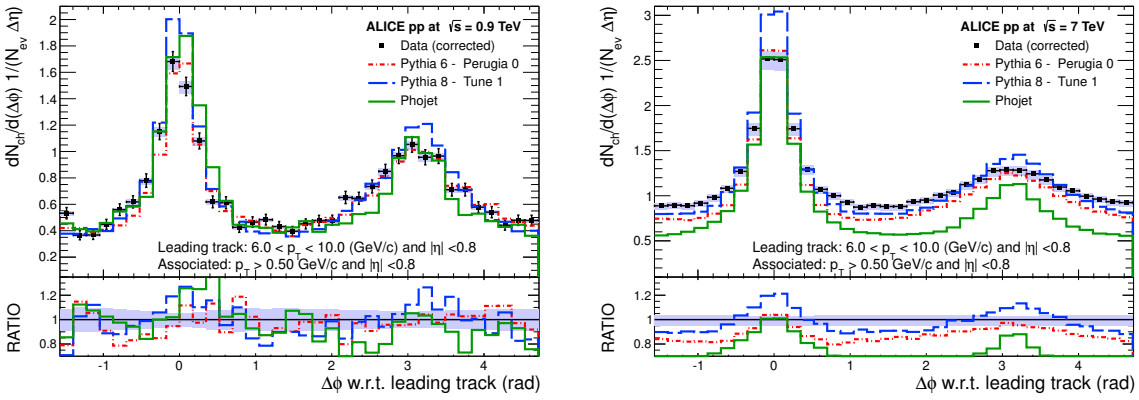

Figure 19. Azimuthal correlation at $\sqrt{s} = 0.9\,\text{TeV}$ (left) and $\sqrt{s} = 7\,\text{TeV}$ (right). Leading-track: $6.0 < p_{T,LT} < 10.0\,\text{GeV}/c$. For visualization purposes the $\Delta\phi$ axis is not centered around 0. Shaded area in upper plots: systematic uncertainties. Shaded areas in bottom plots: sum in quadrature of statistical and systematic uncertainties. Horizontal error bars: bin width.

JHEP07(2012)116

Azimuthal correlations — track $p_{\mathrm{T}} > 1.0\,\mathrm{GeV}/c$.

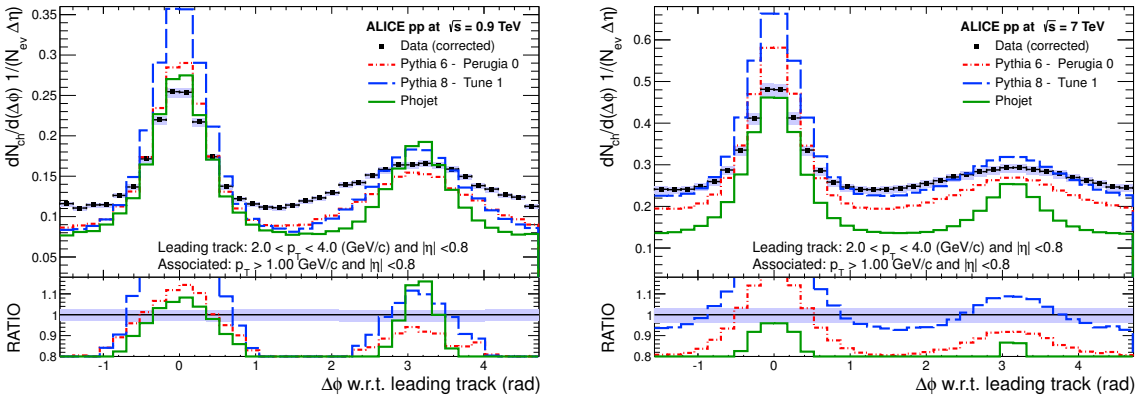

Figure 20. Azimuthal correlation at $\sqrt{s} = 0.9\,\mathrm{TeV}$ (left) and $\sqrt{s} = 7\,\mathrm{TeV}$ (right). Leading-track: $2.0 < p_{T,LT} < 4.0\,\mathrm{GeV}/c$. For visualization purposes the $\Delta\phi$ axis is not centered around 0. Shaded area in upper plots: systematic uncertainties. Shaded areas in bottom plots: sum in quadrature of statistical and systematic uncertainties. Horizontal error bars: bin width.

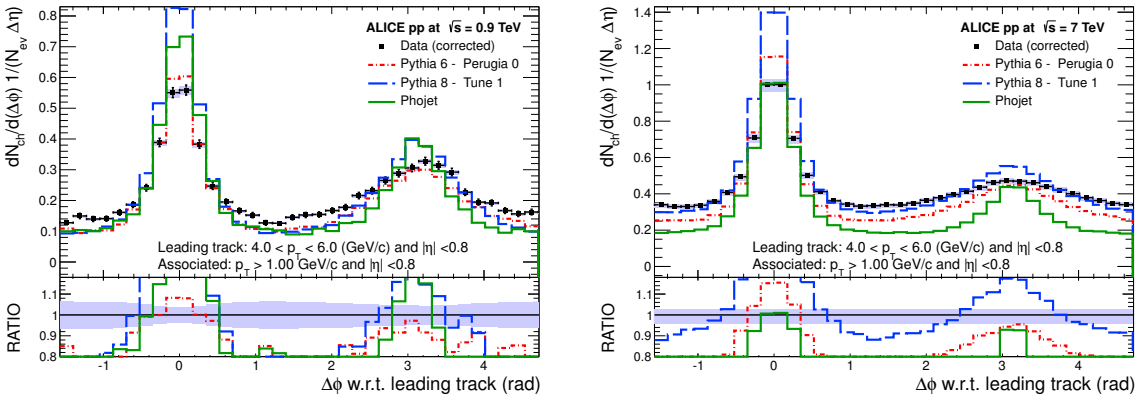

Figure 21. Azimuthal correlation at $\sqrt{s} = 0.9\,\mathrm{TeV}$ (left) and $\sqrt{s} = 7\,\mathrm{TeV}$ (right). Leading-track: $4.0 < p_{T,LT} < 6.0\,\mathrm{GeV}/c$. For visualization purposes the $\Delta\phi$ axis is not centered around 0. Shaded area in upper plots: systematic uncertainties. Shaded areas in bottom plots: sum in quadrature of statistical and systematic uncertainties. Horizontal error bars: bin width.

JHEP07(2012)116

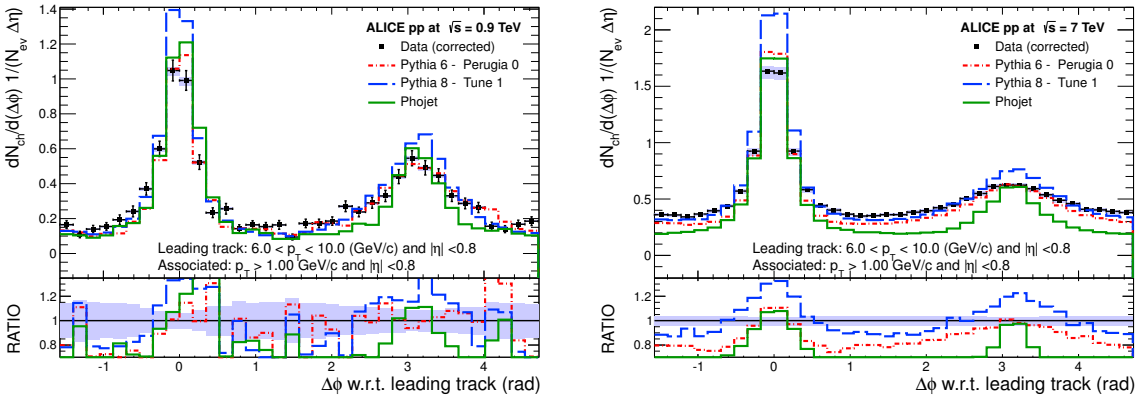

Figure 22. Azimuthal correlation at $\sqrt{s} = 0.9\,\text{TeV}$ (left) and $\sqrt{s} = 7\,\text{TeV}$ (right). Leading-track: $6.0 < p_{T,LT} < 10.0\,\text{GeV}/c$. For visualization purposes the $\Delta\phi$ axis is not centered around 0. Shaded area in upper plots: systematic uncertainties. Shaded areas in bottom plots: sum in quadrature of statistical and systematic uncertainties. Horizontal error bars: bin width.

Acknowledgments

The ALICE collaboration would like to thank all its engineers and technicians for their invaluable contributions to the construction of the experiment and the CERN accelerator teams for the outstanding performance of the LHC complex.

The ALICE collaboration acknowledges the following funding agencies for their support in building and running the ALICE detector: Calouste Gulbenkian Foundation from Lisbon and Swiss Fonds Kidagan, Armenia; Conselho Nacional de Desenvolvimento Científico e Tecnológico (CNPq), Financiadora de Estudos e Projetos (FINEP), Fundação de Amparo à Pesquisa do Estado de São Paulo (FAPESP); National Natural Science Foundation of China (NSFC), the Chinese Ministry of Education (CMOE) and the Ministry of Science and Technology of China (MSTC); Ministry of Education and Youth of the Czech Republic; Danish Natural Science Research Council, the Carlsberg Foundation and the Danish National Research Foundation; The European Research Council under the European Community's Seventh Framework Programme; Helsinki Institute of Physics and the Academy of Finland; French CNRS-IN2P3, the 'Region Pays de Loire', 'Region Alsace', 'Region Auvergne' and CEA, France; German BMBF and the Helmholtz Association; General Secretariat for Research and Technology, Ministry of Development, Greece; Hungarian OTKA and National Office for Research and Technology (NKTH); Department of Atomic Energy and Department of Science and Technology of the Government of India; Istituto Nazionale di Fisica Nucleare (INFN) of Italy; MEXT Grant-in-Aid for Specially Promoted Research, Japan; Joint Institute for Nuclear Research, Dubna; National Research Foundation of Korea (NRF); CONACYT, DGAPA, México, ALFA-EC and the HELEN Program (High-Energy physics Latin-American-European Network); Stichting voor Fundamenteel Onderzoek der Materie (FOM) and the Nederlandse Organisatie voor Wetenschappelijk Onderzoek (NWO), Netherlands; Research Council of Norway (NFR); Polish Ministry of

JHEP07(2012)116

Science and Higher Education; National Authority for Scientific Research - NASR (Autoritatea Naţională pentru Cercetare Ştiinţifică - ANCS); Federal Agency of Science of the Ministry of Education and Science of Russian Federation, International Science and Technology Center, Russian Academy of Sciences, Russian Federal Agency of Atomic Energy, Russian Federal Agency for Science and Innovations and CERN-INTAS; Ministry of Education of Slovakia; Department of Science and Technology, South Africa; CIEMAT, EELA, Ministerio de Educación y Ciencia of Spain, Xunta de Galicia (Consellería de Educación), CEADEN, Cubaenergía, Cuba, and IAEA (International Atomic Energy Agency); Swedish Reseach Council (VR) and Knut & Alice Wallenberg Foundation (KAW); Ukraine Ministry of Education and Science; United Kingdom Science and Technology Facilities Council (STFC); The United States Department of Energy, the United States National Science Foundation, the State of Texas, and the State of Ohio.

References

[1] T. Sjöstrand and P.Z. Skands, *Multiple interactions and the structure of beam remnants*, *JHEP* **03** (2004) 053 [hep-ph/0402078] [INSPIRE].

[2] CDF collaboration, T. Affolder et al., *Charged jet evolution and the underlying event in $p\bar{p}$ collisions at* 1.8 *TeV*, *Phys. Rev.* **D 65** (2002) 092002 [INSPIRE].

[3] CDF collaboration, D. Acosta et al., *The underlying event in hard interactions at the Tevatron $\bar{p}p$ collider*, *Phys. Rev.* **D 70** (2004) 072002 [hep-ex/0404004] [INSPIRE].

[4] CDF collaboration, R. Field, *Min-bias and the underlying event in Run* 2 *at CDF*, *Acta Phys. Polon.* **B 36** (2005) 167 [INSPIRE].

[5] CDF collaboration, T. Aaltonen et al., *Studying the underlying event in Drell-Yan and high transverse momentum jet production at the Tevatron*, *Phys. Rev.* **D 82** (2010) 034001 [arXiv:1003.3146] [INSPIRE].

[6] H. Caines, *Underlying event studies at RHIC*, arXiv:0910.5203 [INSPIRE].

[7] ATLAS collaboration, G. Aad et al., *Measurement of underlying event characteristics using charged particles in pp collisions at $\sqrt{s} = 900$ GeV and 7 TeV with the ATLAS detector*, *Phys. Rev.* **D 83** (2011) 112001 [arXiv:1012.0791] [INSPIRE].

[8] CMS collaboration, V. Khachatryan et al., *First measurement of the underlying event activity at the LHC with $\sqrt{s} = 0.9$ TeV*, *Eur. Phys. J.* **C 70** (2010) 555 [arXiv:1006.2083] [INSPIRE].

[9] A. Buckley et al., *General-purpose event generators for LHC physics*, *Phys. Rept.* **504** (2011) 145 [arXiv:1101.2599] [INSPIRE].

[10] T. Sjöstrand, S. Mrenna and P.Z. Skands, *PYTHIA* 6.4 *physics and manual*, *JHEP* **05** (2006) 026 [hep-ph/0603175] [INSPIRE].

[11] S. Roesler, R. Engel and J. Ranft, *The Monte Carlo event generator DPMJET-III*, hep-ph/0012252 [INSPIRE].

JHEP07(2012)116

[12] M. Bahr et al., *HERWIG++ physics and manual*, *Eur. Phys. J.* **C 58** (2008) 639 [arXiv:0803.0883] [INSPIRE].

[13] B. Andersson, G. Gustafson, G. Ingelman and T. Sjöstrand, *Parton fragmentation and string dynamics*, *Phys. Rept.* **97** (1983) 31 [INSPIRE].

[14] T. Sjöstrand and P.Z. Skands, *Transverse-momentum-ordered showers and interleaved multiple interactions*, *Eur. Phys. J.* **C 39** (2005) 129 [hep-ph/0408302] [INSPIRE].

[15] T. Sjöstrand, S. Mrenna and P.Z. Skands, *A brief introduction to PYTHIA* 8.1, *Comput. Phys. Commun.* **178** (2008) 852 [arXiv:0710.3820] [INSPIRE].

[16] R. Corke and T. Sjöstrand, *Multiparton interactions and rescattering*, *JHEP* **01** (2010) 035 [arXiv:0911.1909] [INSPIRE].

[17] A. Capella, U. Sukhatme, C.-I. Tan and J. Tran Thanh Van, *Dual parton model*, *Phys. Rept.* **236** (1994) 225 [INSPIRE].

[18] ALICE collaboration, K. Aamodt et al., *First proton-proton collisions at the LHC as observed with the ALICE detector: measurement of the charged particle pseudorapidity density at* $\sqrt{s} = 900$ *GeV*, *Eur. Phys. J.* **C 65** (2010) 111 [arXiv:0911.5430] [INSPIRE].

[19] ALICE collaboration, K. Aamodt et al., *Charged-particle multiplicity measurement in proton-proton collisions at* $\sqrt{s} = 0.9$ *and* 2.36 *TeV with ALICE at LHC*, *Eur. Phys. J.* **C 68** (2010) 89 [arXiv:1004.3034] [INSPIRE].

[20] ALICE collaboration, K. Aamodt et al., *Charged-particle multiplicity measurement in proton-proton collisions at* $\sqrt{s} = 7$ *TeV with ALICE at LHC*, *Eur. Phys. J.* **C 68** (2010) 345 [arXiv:1004.3514] [INSPIRE].

[21] ALICE collaboration, A.K. Aamodt et al., *Midrapidity antiproton-to-proton ratio in pp collisions at* $\sqrt{s} = 0.9$ *and* 7 *TeV measured by the ALICE experiment*, *Phys. Rev. Lett.* **105** (2010) 072002 [arXiv:1006.5432] [INSPIRE].

[22] ALICE collaboration, K. Aamodt et al., *Two-pion Bose-Einstein correlations in central Pb-Pb collisions at* $\sqrt{s_{\rm NN}} = 2.76$ *TeV*, *Phys. Lett.* **B 696** (2011) 328 [arXiv:1012.4035] [INSPIRE].

[23] ALICE collaboration, K. Aamodt et al., *Transverse momentum spectra of charged particles in proton-proton collisions at* $\sqrt{s} = 900$ *GeV with ALICE at the LHC*, *Phys. Lett.* **B 693** (2010) 53 [arXiv:1007.0719] [INSPIRE].

[24] ALICE collaboration, K. Aamodt et al., *Strange particle production in proton-proton collisions at* $\sqrt{s} = 0.9$ *TeV with ALICE at the LHC*, *Eur. Phys. J.* **C 71** (2011) 1594 [arXiv:1012.3257] [INSPIRE].

[25] ALICE collaboration, K. Aamodt et al., *The ALICE experiment at the CERN LHC*, 2008 *JINST* **3** S08002 [INSPIRE].

[26] P.Z. Skands, *Tuning Monte Carlo generators: the Perugia tunes*, *Phys. Rev.* **D 82** (2010) 074018 [arXiv:1005.3457] [INSPIRE].

[27] R. Brun, F. Bruyant, M. Maire, A.C. McPherson and P. Zanarini, *GEANT*3, CERN-DD-EE-84-1, CERN, Geneva Switzerland (1987) [INSPIRE].

[28] ALICE collaboration, K. Aamodt et al., *Alignment of the ALICE inner tracking system with cosmic-ray tracks*, 2010 *JINST* **5** P03003 [arXiv:1001.0502] [INSPIRE].

JHEP07(2012)116

[29] T. Sjöstrand and M. van Zijl, *A multiple interaction model for the event structure in hadron collisions*, *Phys. Rev.* **D 36** (1987) 2019 [INSPIRE].

[30] ATLAS collaboration, *Measurement of underlying event characteristics using charged particles in pp collisions at* $\sqrt{s} = 900$ *GeV and* 7 *TeV with the ATLAS detector in a limited phase space*, ATLAS-CONF-2011-009, CERN, Geneva Switzerland (2011).

[31] CMS collaboration, S. Chatrchyan et al., *Measurement of the underlying event activity at the LHC with* $\sqrt{s} = 7$ *TeV and comparison with* $\sqrt{s} = 0.9$ *TeV*, CERN-PH-EP-2011-059, CERN, Geneva Switzerland (2011) [*JHEP* **09** (2011) 109] [arXiv:1107.0330] [INSPIRE].

[32] ATLAS collaboration, G. Aad et al., *Charged-particle multiplicities in pp interactions measured with the ATLAS detector at the LHC*, *New J. Phys.* **13** (2011) 053033 [arXiv:1012.5104] [INSPIRE].

JHEP07(2012)116

The ALICE collaboration

Betty Abelev,[cq] Arian Abrahantes Quintana,[af] Dagmar Adamova,[cv] Andrew Marshall Adare,[eq] Madan Aggarwal,[cz] Gianluca Aglieri Rinella,[bd] Andras Gabor Agocs,[ch] Andrea Agostinelli,[as] Saul Aguilar Salazar,[cd] Zubayer Ahammed,[em] Nazeer Ahmad,[an] Arshad Ahmad,[an] Sang Un Ahn,[cl,bk] Alexander Akindinov,[bt] Dmitry Aleksandrov,[dk] Bruno Alessandro,[dq] Jose Ruben Alfaro Molina,[cd] Andrea Alici,[dr,bd,ai] Anton Alkin,[ab] Erick Jonathan Almaraz Avina,[cd] Torsten Alt,[bj] Valerio Altini,[bb,bd] Sedat Altinpinar,[ao] Igor Altsybeev,[en] Cristian Andrei,[cs] Anton Andronic,[dh] Venelin Anguelov,[de] Christopher Daniel Anson,[ap] Tome Anticic,[di] Federico Antinori,[dv] Pietro Antonioli,[dr] Laurent Bernard Aphecetche,[dx] Harald Appelshauser,[bz] Nicolas Arbor,[cm] Silvia Arcelli,[as] Andreas Arend,[bz] Nestor Armesto,[am] Roberta Arnaldi,[dq] Tomas Robert Aronsson,[eq] Ionut Cristian Arsene,[dh] Mesut Arslandok,[bz] Andzhey Asryan,[en] Andre Augustinus,[bd] Ralf Peter Averbeck,[dh] Terry Awes,[cw] Juha Heikki Aysto,[bl] Mohd Danish Azmi,[an] Matthias Jakob Bach,[bj] Angela Badala,[ds] Yong Wook Baek,[cl,bk] Raphaelle Marie Bailhache,[bz] Renu Bala,[dq] Rinaldo Baldini Ferroli,[ai] Alberto Baldisseri,[al] Alain Baldit,[cl] Fernando Baltasar Dos Santos Pedrosa,[bd] Jaroslav Ban,[bu] Rama Chandra Baral,[bv] Roberto Barbera,[ax] Francesco Barile,[bb] Gergely Gabor Barnafoldi,[ch] Lee Stuart Barnby,[dm] Valerie Barret,[cl] Jerzy Gustaw Bartke,[ea] Maurizio Basile,[as] Nicole Bastid,[cl] Bastian Bathen,[cb] Guillaume Batigne,[dx] Boris Batyunya,[cg] Christoph Heinrich Baumann,[bz] Ian Gardner Bearden,[ct] Hans Beck,[bz] Iouri Belikov,[cf] Francesca Bellini,[as] Rene Bellwied,[eg] Ernesto Belmont-Moreno,[cd] Stefania Beole,[az] Ionela Berceanu,[cs] Alexandru Bercuci,[cs] Yaroslav Berdnikov,[cx] Daniel Berenyi,[ch] Cyrano Bergmann,[cb] Dario Berzano,[dq] Latchezar Betev,[bd] Anju Bhasin,[dc] Ashok Kumar Bhati,[cz] Nicola Bianchi,[cn] Livio Bianchi,[az] Chiara Bianchin,[av] Jaroslav Bielcik,[bh] Jana Bielcikova,[cv] Ante Bilandzic,[cu] F. Blanco,[ag] Francesco Blanco,[eg] Dmitry Blau,[dk] Christoph Blume,[bz] Marco Boccioli,[bd] Nicolas Bock,[ap] Alexey Bogdanov,[cr] Hans Boggild,[ct] Mikhail Bogolyubsky,[bq] Laszlo Boldizsar,[ch] Marek Bombara,[bi] Julian Book,[bz] Herve Borel,[al] Alexander Borissov,[ep] Claudio Bortolin,[av,ex] Suvendu Nath Bose,[dl] Francesco Bossu,[bd,az] Michiel Botje,[cu] Stefan Bottger,[by] Bruno Alexandre Boyer,[bp] Peter Braun-Munzinger,[dh] Marco Bregant,[dx] Timo Gunther Breitner,[by] Michal Broz,[bg] Rene Brun,[bd] Elena Bruna,[eq,az,dq] Giuseppe Eugenio Bruno,[bb] Dmitry Budnikov,[dj] Henner Buesching,[bz] Stefania Bufalino,[az,dq] Kyrylo Bugaiev,[ab] Oliver Busch,[de] Edith Zinhle Buthelezi,[db] Davide Caffarri,[av] Xu Cai,[bn] Helen Louise Caines,[eq] Ernesto Calvo Villar,[dn] Paolo Camerini,[at] Veronica Canoa Roman,[ah,aa] Giovanni Cara Romeo,[dr] Francesco Carena,[bd] Wisla Carena,[bd] Nelson Carlin Filho,[ed] Federico Carminati,[bd] Camilo Andres Carrillo Montoya,[bd] Amaya Ofelia Casanova Diaz,[cn] Michele Caselle,[bd] Javier Ernesto Castillo Castellanos,[al] Juan Francisco Castillo Hernandez,[dh] Ester Anna Rita Casula,[au] Vasile Catanescu,[cs] Costanza Cavicchioli,[bd] Jan Cepila,[bh] Piergiorgio Cerello,[dq] Beomsu Chang,[bl,et] Sylvain Chapeland,[bd] Jean-Luc Fernand Charvet,[al] Sukalyan Chattopadhyay,[dl] Subhasis Chattopadhyay,[em] Michael Gerard Cherney,[cy] Cvetan Cheshkov,[bd,ef] Brigitte Cheynis,[ef] Emilio Chiavassa,[dq] Vasco Miguel Chibante Barroso,[bd] David Chinellato,[ee] Peter Chochula,[bd] Marek Chojnacki,[bs] Panagiotis Christakoglou,[cu,bs] Christian Holm Christensen,[ct] Peter Christiansen,[bc] Tatsuya Chujo,[ek] Suh-Urk Chung,[dg] Corrado Cicalo,[do]

JHEP07(2012)116

Luisa Cifarelli,[as,bd] Federico Cindolo,[dr] Jean Willy Andre Cleymans,[db] Fabrizio Coccetti,[ai] Jean-Pierre Michel Coffin,[cf] Fabio Colamaria,[bb] Domenico Colella,[bb] Gustavo Conesa Balbastre,[cm] Zaida Conesa del Valle,[bd,cf] Paul Constantin,[de] Giacomo Contin,[at] Jesus Guillermo Contreras,[ah] Thomas Michael Cormier,[ep] Yasser Corrales Morales,[az] Pietro Cortese,[ba] Ismael Cortes Maldonado,[aa] Mauro Rogerio Cosentino,[cp,ee] Filippo Costa,[bd] Manuel Enrique Cotallo,[ag] Elisabetta Crescio,[ah] Philippe Crochet,[cl] Emilia Cruz Alaniz,[cd] Eleazar Cuautle,[cc] Leticia Cunqueiro,[cn] Andrea Dainese,[av,dv] Hans Hjersing Dalsgaard,[ct] Andrea Danu,[bx] Indranil Das,[dl,bp] Kushal Das,[dl] Debasish Das,[dl] Ajay Kumar Dash,[bv,ee] Sadhana Dash,[bo,dq] Sudipan De,[em] Andrea De Azevedo Moregula,[cn] Gabriel de Barros,[ed] Annalisa De Caro,[ay,ai] Giacinto de Cataldo,[dp] Jan de Cuveland,[bj] Alessandro De Falco,[au] Daniele De Gruttola,[ay] Hugues Delagrange,[dx] Eduardo Del Castillo Sanchez,[bd] Andrzej Deloff,[dw] Vyacheslav Demanov,[dj] Nora De Marco,[dq] Ervin Denes,[ch] Salvatore De Pasquale,[ay] Airton Deppman,[ed] Ginevra D'Erasmo,[bb] Raoul Stefan de Rooij,[bs] Domenico Di Bari,[bb] Thomas Dietel,[cb] Carmelo Di Giglio,[bb] Sergio Di Liberto,[du] Antonio Di Mauro,[bd] Pasquale Di Nezza,[cn] Roberto Divia,[bd] Oeystein Djuvsland,[ao] Alexandru Florin Dobrin,[ep,bc] Tadeusz Antoni Dobrowolski,[dw] Isabel Dominguez,[cc] Benjamin Donigus,[dh] Olja Dordic,[ar] Olga Driga,[dx] Anand Kumar Dubey,[em] Laurent Ducroux,[ef] Pascal Dupieux,[cl] Mihir Ranjan Dutta Majumdar,[em] A.K. Dutta Majumdar,[dl] Domenico Elia,[dp] David Philip Emschermann,[cb] Heiko Engel,[by] Hege Austrheim Erdal,[bf] Bruno Espagnon,[bp] Magali Danielle Estienne,[dx] Shinichi Esumi,[ek] David Evans,[dm] Gyulnara Eyyubova,[ar] Daniela Fabris,[av,dv] Julien Faivre,[cm] Davide Falchieri,[as] Alessandra Fantoni,[cn] Markus Fasel,[dh] Roger Worsley Fearick,[db] Anatoly Fedunov,[cg] Dominik Fehlker,[ao] Linus Feldkamp,[cb] Daniel Felea,[bx] Grigory Feofilov,[en] Arturo Fernandez Tellez,[aa] Alessandro Ferretti,[az] Roberta Ferretti,[ba] Jan Figiel,[ea] Marcel Figueredo,[ed] Sergey Filchagin,[dj] Rosa Anna Fini,[dp] Dmitry Finogeev,[br] Fiorella Fionda,[bb] Enrichetta Maria Fiore,[bb] Michele Floris,[bd] Siegfried Valentin Foertsch,[db] Panagiota Foka,[dh] Sergey Fokin,[dk] Enrico Fragiacomo,[dt] Michail Fragkiadakis,[da] Ulrich Michael Frankenfeld,[dh] Ulrich Fuchs,[bd] Christophe Furget,[cm] Mario Fusco Girard,[ay] Jens Joergen Gaardhoje,[ct] Martino Gagliardi,[az] Alberto Gago,[dn] Mauro Gallio,[az] Dhevan Raja Gangadharan,[ap] Paraskevi Ganoti,[cw] Jose Garabatos,[dh] Edmundo Garcia-Solis,[aj] Irakli Garishvili,[cq] Jochen Gerhard,[bj] Marie Germain,[dx] Claudio Geuna,[al] Andrei George Gheata,[bd] Mihaela Gheata,[bd] Bruno Ghidini,[bb] Premomoy Ghosh,[em] Paola Gianotti,[cn] Martin Robert Girard,[eo] Paolo Giubellino,[bd] Ewa Gladysz-Dziadus,[ea] Peter Glassel,[de] Ramon Gomez,[ec] Elena Gonzalez Ferreiro,[am] Laura Helena Gonzalez-Trueba,[cd] Pedro Gonzalez-Zamora,[ag] Sergey Gorbunov,[bj] Ankita Goswami,[dd] Sven Gotovac,[dy] Varlen Grabski,[cd] Lukasz Kamil Graczykowski,[eo] Robert Grajcarek,[de] Alessandro Grelli,[bs] Costin Grigoras,[bd] Alina Gabriela Grigoras,[bd] Vladislav Grigoriev,[cr] Ara Grigoryan,[er] Smbat Grigoryan,[cg] Boris Grinyov,[ab] Nevio Grion,[dt] Philippe Gros,[bc] Jan Fiete Grosse-Oetringhaus,[bd] Jean-Yves Grossiord,[ef] Raffaele Grosso,[bd] Fedor Guber,[br] Rachid Guernane,[cm] Cesar Guerra Gutierrez,[dn] Barbara Guerzoni,[as] Maxime Rene Joseph Guilbaud,[ef] Kristjan Herlache Gulbrandsen,[ct] Taku Gunji,[ej] Anik Gupta,[dc] Ramni Gupta,[dc] Hans Gutbrod,[dh] Oystein Senneset Haaland,[ao] Cynthia Marie Hadjidakis,[bp] Maria Haiduc,[bx] Hideki Hamagaki,[ej] Gergoe Hamar,[ch] Byounghee Han,[aq] Luke David Hanratty,[dm] Alexander Hansen,[ct] Zuzana Harmanova,[bi] John William Harris,[eq]

JHEP07(2012)116

Matthias Hartig,[bz] Dumitru Hasegan,[bx] Despoina Hatzifotiadou,[dr] Arsen Hayrapetyan,[bd,er] Stefan Thomas Heckel,[bz] Markus Ansgar Heide,[cb] Haavard Helstrup,[bf] Andrei Ionut Herghelegiu,[cs] Gerardo Antonio Herrera Corral,[ah] Norbert Herrmann,[de] Kristin Fanebust Hetland,[bf] Bernard Hicks,[eq] Per Thomas Hille,[eq] Boris Hippolyte,[cf] Takuma Horaguchi,[ek] Yasuto Hori,[ej] Peter Zahariev Hristov,[bd] Ivana Hrivnacova,[bp] Meidana Huang,[ao] Sebastian Bernd Huber,[dh] Thomas Humanic,[ap] Dae Sung Hwang,[aq] Raphaelle Ichou,[cl] Radiy Ilkaev,[dj] Iryna Ilkiv,[dw] Motoi Inaba,[ek] Elisa Incani,[au] Pier Giorgio Innocenti,[bd] Gian Michele Innocenti,[az] Mikhail Ippolitov,[dk] Muhammad Irfan,[an] Cristian George Ivan,[dh] Marian Ivanov,[dh] Vladimir Ivanov,[cx] Andrey Ivanov,[en] Oleksii Ivanytskyi,[ab] Adam Wlodzimierz Jacholkowski,[bd] Peter Jacobs,[cp] Lucia Jancurova,[cg] Haeng Jin Jang,[ck] Swensy Gwladys Jangal,[cf] Rudolf Janik,[bg] Malgorzata Anna Janik,[eo] Sandun Jayarathna,[eg] Satyajit Jena,[bo] Raul Tonatiuh Jimenez Bustamante,[cc] Lennart Jirden,[bd] Peter Graham Jones,[dm] Won Woong Jung,[bk] Hyung Taik Jung,[bk] Anton Jusko,[dm] Alexei Kaidalov,[bt] Vanik Kakoyan,[er] Sebastian Kalcher,[bj] Peter Kalinak,[bu] Matus Kalisky,[cb] Tuomo Esa Aukusti Kalliokoski,[bl] Alexander Philipp Kalweit,[ca] Kalliopi Kanaki,[ao] Ju Hwan Kang,[et] Vladimir Kaplin,[cr] Ayben Karasu Uysal,[bd,es] Oleg Karavichev,[br] Tatiana Karavicheva,[br] Evgeny Karpechev,[br] Andrey Kazantsev,[dk] Udo Wolfgang Kebschull,[cj,by] Ralf Keidel,[eu] Palash Khan,[dl] Mohisin Mohammed Khan,[an] Shuaib Ahmad Khan,[em] Alexei Khanzadeev,[cx] Yury Kharlov,[bq] Bjarte Kileng,[bf] Jonghyun Kim,[aq] Dong Jo Kim,[bl] Do Won Kim,[bk] Jin Sook Kim,[bk] Minwoo Kim,[et] Seon Hee Kim,[bk] Se Yong Kim,[aq] Beomkyu Kim,[et] Taesoo Kim,[et] Stefan Kirsch,[bj,bd] Ivan Kisel,[bj] Sergey Kiselev,[bt] Adam Ryszard Kisiel,[bd,eo] Jennifer Lynn Klay,[ad] Jochen Klein,[de] Christian Klein-Bosing,[cb] Michael Kliemant,[bz] Alexander Kluge,[bd] Michael Linus Knichel,[dh] Kathrin Koch,[de] Markus Kohler,[dh] Anatoly Kolojvari,[en] Valery Kondratiev,[en] Natalia Kondratyeva,[cr] Artem Konevskih,[br] Andrey Korneev,[dj] Chamath Kottachchi Kankanamge Don,[ep] Ravjeet Kour,[dm] Marek Kowalski,[ea] Serge Kox,[cm] Greeshma Koyithatta Meethaleveedu,[bo] Jiri Kral,[bl] Ivan Kralik,[bu] Frederick Kramer,[bz] Ingrid Christine Kraus,[dh] Tobias Krawutschke,[de,be] Matthias Kretz,[bj] Marian Krivda,[dm,bu] Filip Krizek,[bl] Miroslav Krus,[bh] Evgeny Kryshen,[cx] Mikolaj Krzewicki,[cu,dh] Yury Kucheriaev,[dk] Christian Claude Kuhn,[cf] Paul Kuijer,[cu] Podist Kurashvili,[dw] A.B. Kurepin,[br] A. Kurepin,[br] Alexey Kuryakin,[dj] Svetlana Kushpil,[cv] Vasily Kushpil,[cv] Henning Kvaerno,[ar] Min Jung Kweon,[de] Youngil Kwon,[et] Pedro Ladron de Guevara,[cc] Igor Lakomov,[bp,en] Rune Langoy,[ao] Camilo Ernesto Lara,[by] Antoine Xavier Lardeux,[dx] Paola La Rocca,[ax] Cristina Lazzeroni,[dm] Ramona Lea,[at] Yves Le Bornec,[bp] Sung Chul Lee,[bk] Ki Sang Lee,[bk] Frederic Lefevre,[dx] Joerg Walter Lehnert,[bz] Lars Leistam,[bd] Matthieu Laurent Lenhardt,[dx] Vito Lenti,[dp] Hermes Leon,[cd] Ildefonso Leon Monzon,[ec] Hermes Leon Vargas,[bz] Peter Levai,[ch] Xiaomei Li,[ak] Jorgen Lien,[ao] Roman Lietava,[dm] Svein Lindal,[ar] Volker Lindenstruth,[bj] Christian Lippmann,[dh,bd] Michael Annan Lisa,[ap] Lijiao Liu,[ao] Per-Ivar Loenne,[ao] Vera Loggins,[ep] Vitaly Loginov,[cr] Stefan Bernhard Lohn,[bd] Daniel Lohner,[de] Constantinos Loizides,[cp] Kai Krister Loo,[bl] Xavier Bernard Lopez,[cl] Ernesto Lopez Torres,[af] Gunnar Lovhoiden,[ar] Xianguo Lu,[de] Philipp Luettig,[bz] Marcello Lunardon,[av] Jiebin Luo,[bn] Grazia Luparello,[bs] Lionel Luquin,[dx] Cinzia Luzzi,[bd] Rongrong Ma,[eq] Ke Ma,[bn] Dilan Minthaka Madagodahettige-Don,[eg] Alla Maevskaya,[br] Magnus Mager,[ca,bd] Durga Prasad Mahapatra,[bv] Antonin Maire,[cf] Mikhail Malaev,[cx]

JHEP07(2012)116

Ivonne Alicia Maldonado Cervantes,[cc] Ludmila Malinina,[cg,ew] Dmitry Mal'Kevich,[bt] Peter Malzacher,[dh] Alexander Mamonov,[dj] Loic Henri Antoine Manceau,[dq] Lalit Kumar Mangotra,[dc] Vladislav Manko,[dk] Franck Manso,[cl] Vito Manzari,[dp] Yaxian Mao,[cm,bn] Massimiliano Marchisone,[cl,az] Jiri Mares,[bw] Giacomo Vito Margagliotti,[at,dt] Anselmo Margotti,[dr] Ana Maria Marin,[dh] Christina Markert,[eb] Irakli Martashvili,[ei] Paolo Martinengo,[bd] Mario Ivan Martinez,[aa] Arnulfo Martinez Davalos,[cd] Gines Martinez Garcia,[dx] Yevgen Martynov,[ab] Alexis Jean-Michel Mas,[dx] Silvia Masciocchi,[dh] Massimo Masera,[az] Alberto Masoni,[do] Laure Marie Massacrier,[ef] Mario Mastromarco,[dp] Annalisa Mastroserio,[bb,bd] Zoe Louise Matthews,[dm] Adam Tomasz Matyja,[dx] Daniel Mayani,[cc] Christoph Mayer,[ea] Joel Mazer,[ei] Alessandra Maria Mazzoni,[du] Franco Meddi,[aw] Arturo Alejandro Menchaca-Rocha,[cd] Jorge Mercado Perez,[de] Michal Meres,[bg] Yasuo Miake,[ek] Alain Michalon,[cf] Jumpei Midori,[bm] Leonardo Milano,[az] Jovan Milosevic,[ar,ex] Andre Mischke,[bs] Aditya Nath Mishra,[dd] Dariusz Miskowiec,[dh,bd] Ciprian Mihai Mitu,[bx] Jocelyn Mlynarz,[ep] Ajit Kumar Mohanty,[bd] Bedangadas Mohanty,[em] Levente Molnar,[bd] Luis Manuel Montano Zetina,[ah] Marco Monteno,[dq] Esther Montes,[ag] Taebong Moon,[et] Maurizio Morando,[av] Denise Aparecida Moreira De Godoy,[ed] Sandra Moretto,[av] Andreas Morsch,[bd] Valeria Muccifora,[cn] Eugen Mudnic,[dy] Sanjib Muhuri,[em] Hans Muller,[bd] Marcelo Munhoz,[ed] Luciano Musa,[bd] Alfredo Musso,[dq] Basanta Kumar Nandi,[bo] Rosario Nania,[dr] Eugenio Nappi,[dp] Christine Nattrass,[ei] Nikolay Naumov,[dj] Sparsh Navin,[dm] Tapan Kumar Nayak,[em] Sergey Nazarenko,[dj] Gleb Nazarov,[dj] Alexander Nedosekin,[bt] Maria Nicassio,[bb] Borge Svane Nielsen,[ct] Takafumi Niida,[ek] Sergey Nikolaev,[dk] Vedran Nikolic,[di] Vladimir Nikulin,[cx] Sergey Nikulin,[dk] Bjorn Steven Nilsen,[cy] Mads Stormo Nilsson,[ar] Francesco Noferini,[dr,ai] Petr Nomokonov,[cg] Gerardus Nooren,[bs] Norbert Novitzky,[bl] Alexandre Nyanin,[dk] Anitha Nyatha,[bo] Casper Nygaard,[ct] Joakim Ingemar Nystrand,[ao] Hideyuki Obayashi,[bm] Alexander Ochirov,[en] Helmut Oskar Oeschler,[ca,bd] Sun Kun Oh,[bk] Saehanseul Oh,[eq] Janusz Oleniacz,[eo] Chiara Oppedisano,[dq] Antonio Ortiz Velasquez,[cc] Giacomo Ortona,[bd,az] Anders Nils Erik Oskarsson,[bc] Piotr Krystian Ostrowski,[eo] Ingvar Otterlund,[bc] Jacek Tomasz Otwinowski,[dh] Ken Oyama,[de] Kyoichiro Ozawa,[ej] Yvonne Chiara Pachmayer,[de] Milos Pachr,[bh] Fatima Padilla,[az] Paola Pagano,[ay] Guy Paic,[cc] Florian Painke,[bj] Carlos Pajares,[am] S. Pal,[al] Susanta Kumar Pal,[em] Arvinder Singh Palaha,[dm] Armando Palmeri,[ds] Vardanush Papikyan,[er] Giuseppe Pappalardo,[ds] Woo Jin Park,[dh] Annika Passfeld,[cb] Blahoslav Pastircak,[bu] Dmitri Ivanovich Patalakha,[bq] Vincenzo Paticchio,[dp] Alexei Pavlinov,[ep] Tomasz Jan Pawlak,[eo] Thomas Peitzmann,[bs] Marianela Perales,[aj] Elienos Pereira De Oliveira Filho,[ed] Dmitri Peresunko,[dk] Carlos Eugenio Perez Lara,[cu] Edgar Perez Lezama,[cc] Diego Perini,[bd] Davide Perrino,[bb] Wiktor Stanislaw Peryt,[eo] Alessandro Pesci,[dr] Vladimir Peskov,[bd,cc] Yury Pestov,[ac] Vojtech Petracek,[bh] Michal Petran,[bh] Mariana Petris,[cs] Plamen Rumenov Petrov,[dm] Mihai Petrovici,[cs] Catia Petta,[ax] Stefano Piano,[dt] Anna Piccotti,[dq] Miroslav Pikna,[bg] Philippe Pillot,[dx] Ombretta Pinazza,[bd] Lawrence Pinsky,[eg] Nora Pitz,[bz] Francois Piuz,[bd] Danthasinghe Piyarathna,[eg] Mateusz Andrzej Ploskon,[cp] Jan Marian Pluta,[eo] Timur Pocheptsov,[cg,ar] Sona Pochybova,[ch] Pedro Luis Manuel Podesta Lerma,[ec] Martin Poghosyan,[bd,az] Karel Polak,[bw] Boris Polichtchouk,[bq] Amalia Pop,[cs] Sarah Porteboeuf-Houssais,[cl] Vladimir Pospisil,[bh] Baba Potukuchi,[dc] Sidharth Kumar Prasad,[ep] Roberto Preghenella,[dr,ai] Francesco Prino,[dq] Claude Andre Pruneau,[ep] Igor Pshenichnov,[br]

JHEP07(2012)116

Sergey Puchagin,[dj] Giovanna Puddu,[au] Alberto Pulvirenti,[ax,bd] Valery Punin,[dj] Marian Putis,[bi] Jorn Henning Putschke,[ep,eq] Emanuele Quercigh,[bd] Henrik Qvigstad,[ar] Alexandre Rachevski,[dt] Alphonse Rademakers,[bd] Sylwester Radomski,[de] Tomi Samuli Raiha,[bl] Jan Rak,[bl] Andry Malala Rakotozafindrabe,[al] Luciano Ramello,[ba] Abdiel Ramirez Reyes,[ah] Sudhir Raniwala,[dd] Rashmi Raniwala,[dd] Sami Sakari Rasanen,[bl] Bogdan Theodor Rascanu,[bz] Deepika Rathee,[cz] Kenneth Francis Read,[ei] Jean-Sebastien Real,[cm] Krzysztof Redlich,[dw,ce] Patrick Reichelt,[bz] Martijn Reicher,[bs] Rainer Arno Ernst Renfordt,[bz] Anna Rita Reolon,[cn] Andrey Reshetin,[br] Felix Vincenz Rettig,[bj] Jean-Pierre Revol,[bd] Klaus Johannes Reygers,[de] Lodovico Riccati,[dq] Renato Angelo Ricci,[co] Matthias Rudolph Richter,[ar] Petra Riedler,[bd] Werner Riegler,[bd] Francesco Riggi,[ax,ds] Mario Rodriguez Cahuantzi,[aa] David Rohr,[bj] Dieter Rohrich,[ao] Rosa Romita,[dh] Federico Ronchetti,[cn] Philippe Rosnet,[cl] Stefan Rossegger,[bd] Andrea Rossi,[av] Filimon Roukoutakis,[da] Pradip Kumar Roy,[dl] Christelle Sophie Roy,[cf] Antonio Juan Rubio Montero,[ag] Rinaldo Rui,[at] Evgeny Ryabinkin,[dk] Andrzej Rybicki,[ea] Sergey Sadovsky,[bq] Karel Safarik,[bd] Pradip Kumar Sahu,[bv] Jogender Saini,[em] Hiroaki Sakaguchi,[bm] Shingo Sakai,[cp] Dosatsu Sakata,[ek] Carlos Albert Salgado,[am] Sanjeev Singh Sambyal,[dc] Vladimir Samsonov,[cx] Xitzel Sanchez Castro,[cc,cf] Ladislav Sandor,[bu] Andres Sandoval,[cd] Masato Sano,[ek] Satoshi Sano,[ej] Rainer Santo,[cb] Romualdo Santoro,[dp,bd] Juho Jaako Sarkamo,[bl] Eugenio Scapparone,[dr] Fernando Scarlassara,[av] Rolf Paul Scharenberg,[df] Claudiu Cornel Schiaua,[cs] Rainer Martin Schicker,[de] Christian Joachim Schmidt,[dh] Hans Rudolf Schmidt,[dh,el] Steffen Schreiner,[bd] Simone Schuchmann,[bz] Jurgen Schukraft,[bd] Yves Roland Schutz,[bd,dx] Kilian Eberhard Schwarz,[dh] Kai Oliver Schweda,[dh,de] Gilda Scioli,[as] Enrico Scomparin,[dq] Rebecca Scott,[ei] Patrick Aaron Scott,[dm] Gianfranco Segato,[av] Ilya Selioujenkov,[dh] Serhiy Senyukov,[ba,cf] Jeewon Seo,[dg] Sergio Serci,[au] Eulogio Serradilla,[ag,cd] Adrian Sevcenco,[bx] Irene Sgura,[dp] Alexandre Shabetai,[dx] Galina Shabratova,[cg] Ruben Shahoyan,[bd] Natasha Sharma,[cz] Satish Sharma,[dc] Kenta Shigaki,[bm] Maya Shimomura,[ek] Katherin Shtejer,[af] Yury Sibiriak,[dk] Melinda Siciliano,[az] Eva Sicking,[bd] Sabyasachi Siddhanta,[do] Teodor Siemiarczuk,[dw] David Olle Rickard Silvermyr,[cw] Giuseppe Simonetti,[bb,bd] Rama Narayana Singaraju,[em] Ranbir Singh,[dc] Subhash Singha,[em] Bikash Sinha,[em] Tinku Sinha,[dl] Branislav Sitar,[bg] Mario Sitta,[ba] Bernhard Skaali,[ar] Kyrre Skjerdal,[ao] Radek Smakal,[bh] Nikolai Smirnov,[eq] Raimond Snellings,[bs] Carsten Sogaard,[ct] Ron Ariel Soltz,[cq] Hyungsuk Son,[aq] Jihye Song,[dg] Myunggeun Song,[et] Csaba Soos,[bd] Francesca Soramel,[av] Iwona Sputowska,[ea] Martha Spyropoulou-Stassinaki,[da] Brijesh Kumar Srivastava,[df] Johanna Stachel,[de] Ionel Stan,[bx] Ionel Stan,[bx] Grzegorz Stefanek,[dw] Giorgio Stefanini,[bd] Timm Morten Steinbeck,[bj] Matthew Steinpreis,[ap] Evert Anders Stenlund,[bc] Gideon Francois Steyn,[db] Diego Stocco,[dx] Mikhail Stolpovskiy,[bq] Kirill Strabykin,[dj] Peter Strmen,[bg] Alexandre Alarcon do Passo Suaide,[ed] Martin Alfonso Subieta Vasquez,[az] Toru Sugitate,[bm] Christophe Pierre Suire,[bp] Mikhail Sukhorukov,[dj] Rishat Sultanov,[bt] Michal Sumbera,[cv] Tatjana Susa,[di] Alejandro Szanto de Toledo,[ed] Imrich Szarka,[bg] Artur Krzysztof Szostak,[ao] Christos Tagridis,[da] Jun Takahashi,[ee] Daniel Jesus Tapia Takaki,[bp] Arturo Tauro,[bd] Guillermo Tejeda Munoz,[aa] Adriana Telesca,[bd] Cristina Terrevoli,[bb] Jochen Mathias Thader,[dh] Jim Thomas,[dh] Deepa Thomas,[bs] Raphael Noel Tieulent,[ef] Anthony Timmins,[eg] David Tlusty,[bh] Alberica Toia,[bj,bd] Hisayuki Torii,[bm,ej] Luca Toscano,[dq] Flavio Tosello,[dq] Tomasz Traczyk,[eo] David Christopher Truesdale,[ap]

JHEP07(2012)116

Wladyslaw Henryk Trzaska,[bl] Tomoya Tsuji,[ej] Alexandr Tumkin,[dj] Rosario Turrisi,[dv] Trine Spedstad Tveter,[ar] Jason Glyndwr Ulery,[bz] Kjetil Ullaland,[ao] Jochen Ulrich,[cj,by] Antonio Uras,[ef] Jozef Urban,[bi] Guido Marie Urciuoli,[du] Gianluca Usai,[au] Michal Vajzer,[bh,cv] Martin Vala,[cg,bu] Lizardo Valencia Palomo,[bp] Sara Vallero,[de] Naomi van der Kolk,[cu] Pierre Vande Vyvre,[bd] Marco van Leeuwen,[bs] Luigi Vannucci,[co] Aurora Diozcora Vargas,[aa] Raghava Varma,[bo] Maria Vasileiou,[da] Andrey Vasiliev,[dk] Vladimir Vechernin,[en] Misha Veldhoen,[bs] Massimo Venaruzzo,[at] Ermanno Vercellin,[az] Sergio Vergara,[aa] Don Constantin Vernekohl,[cb] Renaud Vernet,[ae] Marta Verweij,[bs] Linda Vickovic,[dy] Giuseppe Viesti,[av] Oleg Vikhlyantsev,[dj] Zabulon Vilakazi,[db] Orlando Villalobos Baillie,[dm] Leonid Vinogradov,[en] Yury Vinogradov,[dj] Alexander Vinogradov,[dk] Tiziano Virgili,[ay] Yogendra Viyogi,[em] Alexander Vodopianov,[cg] Sergey Voloshin,[ep] Kirill Voloshin,[bt] Giacomo Volpe,[bb,bd] Barthelemy von Haller,[bd] Danilo Vranic,[dh] Gaute vrebekk,[ao] Janka Vrlakova,[bi] Bogdan Vulpescu,[cl] Alexey Vyushin,[dj] Boris Wagner,[ao] Vladimir Wagner,[bh] Renzhuo Wan,[cf,bn] Yifei Wang,[de] Mengliang Wang,[bn] Dong Wang,[bn] Yaping Wang,[bn] Kengo Watanabe,[ek] Johannes Wessels,[bd,cb] Uwe Westerhoff,[cb] Jens Wiechula,[de,el] Jon Wikne,[ar] Martin Rudolf Wilde,[cb] Grzegorz Andrzej Wilk,[dw] Alexander Wilk,[cb] Crispin Williams,[dr] Bernd Stefan Windelband,[de] Leonidas Xaplanteris Karampatsos,[eb] Hongyan Yang,[al] Shiming Yang,[ao] Satoshi Yano,[bm] Stanislav Yasnopolsky,[dk] JunGyu Yi,[dg] Zhongbao Yin,[bn] Hiroki Yokoyama,[ek] In-Kwon Yoo,[dg] Jongik Yoon,[et] Weilin Yu,[bz] Xianbao Yuan,[bn] Igor Yushmanov,[dk] Cenek Zach,[bh] Chiara Zampolli,[dr,bd] Sergey Zaporozhets,[cg] Andrey Zarochentsev,[en] Petr Zavada,[bw] Nikolai Zaviyalov,[dj] Hanna Paulina Zbroszczyk,[eo] Pierre Zelnicek,[bd,by] Sorin Ion Zgura,[bx] Mikhail Zhalov,[cx] Xiaoming Zhang,[cl,bn] Fengchu Zhou,[bn] You Zhou,[bs] Daicui Zhou,[bn] Xiangrong Zhu,[bn] Antonino Zichichi,[as,ai] Alice Zimmermann,[de] Gennady Zinovjev,[ab] Yannick Denis Zoccarato[ef] and Mykhaylo Zynovyev[ab]

aa: Benemérita Universidad Autónoma de Puebla, Puebla, Mexico
ab: Bogolyubov Institute for Theoretical Physics, Kiev, Ukraine
ac: Budker Institute for Nuclear Physics, Novosibirsk, Russia
ad: California Polytechnic State University, San Luis Obispo, California, United States
ae: Centre de Calcul de l'IN2P3, Villeurbanne, France
af: Centro de Aplicaciones Tecnológicas y Desarrollo Nuclear (CEADEN), Havana, Cuba
ag: Centro de Investigaciones Energéticas Medioambientales y Tecnológicas (CIEMAT), Madrid, Spain
ah: Centro de Investigación y de Estudios Avanzados (CINVESTAV), Mexico City and Mérida, Mexico
ai: Centro Fermi — Centro Studi e Ricerche e Museo Storico della Fisica "Enrico Fermi", Rome, Italy
aj: Chicago State University, Chicago, United States
ak: China Institute of Atomic Energy, Beijing, China
al: Commissariat à l'Energie Atomique, IRFU, Saclay, France
am: Departamento de Física de Partículas and IGFAE, Universidad de Santiago de Compostela, Santiago de Compostela, Spain
an: Department of Physics Aligarh Muslim University, Aligarh, India
ao: Department of Physics and Technology, University of Bergen, Bergen, Norway

JHEP07(2012)116

ap: Department of Physics, Ohio State University, Columbus, Ohio, United States
aq: Department of Physics, Sejong University, Seoul, South Korea
ar: Department of Physics, University of Oslo, Oslo, Norway
as: Dipartimento di Fisica dell'Università and Sezione INFN, Bologna, Italy
at: Dipartimento di Fisica dell'Università and Sezione INFN, Trieste, Italy
au: Dipartimento di Fisica dell'Università and Sezione INFN, Cagliari, Italy
av: Dipartimento di Fisica dell'Università and Sezione INFN, Padova, Italy
aw: Dipartimento di Fisica dell'Università 'La Sapienza' and Sezione INFN, Rome, Italy
ax: Dipartimento di Fisica e Astronomia dell'Università and Sezione INFN, Catania, Italy
ay: Dipartimento di Fisica 'E.R. Caianiello' dell'Università and Gruppo Collegato INFN, Salerno, Italy
az: Dipartimento di Fisica Sperimentale dell'Università and Sezione INFN, Turin, Italy
ba: Dipartimento di Scienze e Tecnologie Avanzate dell'Università del Piemonte Orientale and Gruppo Collegato INFN, Alessandria, Italy
bb: Dipartimento Interateneo di Fisica 'M. Merlin' and Sezione INFN, Bari, Italy
bc: Division of Experimental High Energy Physics, University of Lund, Lund, Sweden
bd: European Organization for Nuclear Research (CERN), Geneva, Switzerland
be: Fachhochschule Köln, Köln, Germany
bf: Faculty of Engineering, Bergen University College, Bergen, Norway
bg: Faculty of Mathematics, Physics and Informatics, Comenius University, Bratislava, Slovakia
bh: Faculty of Nuclear Sciences and Physical Engineering, Czech Technical University in Prague, Prague, Czech Republic
bi: Faculty of Science, P.J. Šafárik University, Košice, Slovakia
bj: Frankfurt Institute for Advanced Studies, Johann Wolfgang Goethe-Universität Frankfurt, Frankfurt, Germany
bk: Gangneung-Wonju National University, Gangneung, South Korea
bl: Helsinki Institute of Physics (HIP) and University of Jyväskylä, Jyväskylä, Finland
bm: Hiroshima University, Hiroshima, Japan
bn: Hua-Zhong Normal University, Wuhan, China
bo: Indian Institute of Technology, Mumbai, India
bp: Institut de Physique Nucléaire d'Orsay (IPNO), Université Paris-Sud, CNRS-IN2P3, Orsay, France
bq: Institute for High Energy Physics, Protvino, Russia
br: Institute for Nuclear Research, Academy of Sciences, Moscow, Russia
bs: Nikhef, National Institute for Subatomic Physics and Institute for Subatomic Physics of Utrecht University, Utrecht, Netherlands
bt: Institute for Theoretical and Experimental Physics, Moscow, Russia
bu: Institute of Experimental Physics, Slovak Academy of Sciences, Košice, Slovakia
bv: Institute of Physics, Bhubaneswar, India
bw: Institute of Physics, Academy of Sciences of the Czech Republic, Prague, Czech Republic
bx: Institute of Space Sciences (ISS), Bucharest, Romania
by: Institut für Informatik, Johann Wolfgang Goethe-Universität Frankfurt, Frankfurt, Germany
bz: Institut für Kernphysik, Johann Wolfgang Goethe-Universität Frankfurt, Frankfurt, Germany
ca: Institut für Kernphysik, Technische Universität Darmstadt, Darmstadt, Germany
cb: Institut für Kernphysik, Westfälische Wilhelms-Universität Münster, Münster, Germany
cc: Instituto de Ciencias Nucleares, Universidad Nacional Autónoma de México, Mexico City, Mexico
cd: Instituto de Física, Universidad Nacional Autónoma de México, Mexico City, Mexico

JHEP07(2012)116

ce: Institut of Theoretical Physics, University of Wroclaw
cf: Institut Pluridisciplinaire Hubert Curien (IPHC), Université de Strasbourg, CNRS-IN2P3, Strasbourg, France
cg: Joint Institute for Nuclear Research (JINR), Dubna, Russia
ch: KFKI Research Institute for Particle and Nuclear Physics, Hungarian Academy of Sciences, Budapest, Hungary
ci: Kharkiv Institute of Physics and Technology (KIPT), National Academy of Sciences of Ukraine (NASU), Kharkov, Ukraine
cj: Kirchhoff-Institut für Physik, Ruprecht-Karls-Universität Heidelberg, Heidelberg, Germany
ck: Korea Institute of Science and Technology Information
cl: Laboratoire de Physique Corpusculaire (LPC), Clermont Université, Université Blaise Pascal, CNRS-IN2P3, Clermont-Ferrand, France
cm: Laboratoire de Physique Subatomique et de Cosmologie (LPSC), Université Joseph Fourier, CNRS-IN2P3, Institut Polytechnique de Grenoble, Grenoble, France
cn: Laboratori Nazionali di Frascati, INFN, Frascati, Italy
co: Laboratori Nazionali di Legnaro, INFN, Legnaro, Italy
cp: Lawrence Berkeley National Laboratory, Berkeley, California, United States
cq: Lawrence Livermore National Laboratory, Livermore, California, United States
cr: Moscow Engineering Physics Institute, Moscow, Russia
cs: National Institute for Physics and Nuclear Engineering, Bucharest, Romania
ct: Niels Bohr Institute, University of Copenhagen, Copenhagen, Denmark
cu: Nikhef, National Institute for Subatomic Physics, Amsterdam, Netherlands
cv: Nuclear Physics Institute, Academy of Sciences of the Czech Republic, Řež u Prahy, Czech Republic
cw: Oak Ridge National Laboratory, Oak Ridge, Tennessee, United States
cx: Petersburg Nuclear Physics Institute, Gatchina, Russia
cy: Physics Department, Creighton University, Omaha, Nebraska, United States
cz: Physics Department, Panjab University, Chandigarh, India
da: Physics Department, University of Athens, Athens, Greece
db: Physics Department, University of Cape Town, iThemba LABS, Cape Town, South Africa
dc: Physics Department, University of Jammu, Jammu, India
dd: Physics Department, University of Rajasthan, Jaipur, India
de: Physikalisches Institut, Ruprecht-Karls-Universität Heidelberg, Heidelberg, Germany
df: Purdue University, West Lafayette, Indiana, United States
dg: Pusan National University, Pusan, South Korea
dh: Research Division and ExtreMe Matter Institute EMMI, GSI Helmholtzzentrum für Schwerionenforschung, Darmstadt, Germany
di: Rudjer Bošković Institute, Zagreb, Croatia
dj: Russian Federal Nuclear Center (VNIIEF), Sarov, Russia
dk: Russian Research Centre Kurchatov Institute, Moscow, Russia
dl: Saha Institute of Nuclear Physics, Kolkata, India
dm: School of Physics and Astronomy, University of Birmingham, Birmingham, United Kingdom
dn: Sección Física, Departamento de Ciencias, Pontificia Universidad Católica del Perú, Lima, Peru
do: Sezione INFN, Cagliari, Italy
dp: Sezione INFN, Bari, Italy
dq: Sezione INFN, Turin, Italy
dr: Sezione INFN, Bologna, Italy

JHEP07(2012)116

ds: Sezione INFN, Catania, Italy
dt: Sezione INFN, Trieste, Italy
du: Sezione INFN, Rome, Italy
dv: Sezione INFN, Padova, Italy
dw: Soltan Institute for Nuclear Studies, Warsaw, Poland
dx: SUBATECH, Ecole des Mines de Nantes, Université de Nantes, CNRS-IN2P3, Nantes, France
dy: Technical University of Split FESB, Split, Croatia
ea: The Henryk Niewodniczanski Institute of Nuclear Physics, Polish Academy of Sciences, Cracow, Poland
eb: The University of Texas at Austin, Physics Department, Austin, TX, United States
ec: Universidad Autónoma de Sinaloa, Culiacán, Mexico
ed: Universidade de São Paulo (USP), São Paulo, Brazil
ee: Universidade Estadual de Campinas (UNICAMP), Campinas, Brazil
ef: Université de Lyon, Université Lyon 1, CNRS/IN2P3, IPN-Lyon, Villeurbanne, France
eg: University of Houston, Houston, Texas, United States
eh: University of Technology and Austrian Academy of Sciences, Vienna, Austria
ei: University of Tennessee, Knoxville, Tennessee, United States
ej: University of Tokyo, Tokyo, Japan
ek: University of Tsukuba, Tsukuba, Japan
el: Eberhard Karls Universität Tübingen, Tübingen, Germany
em: Variable Energy Cyclotron Centre, Kolkata, India
en: V. Fock Institute for Physics, St. Petersburg State University, St. Petersburg, Russia
eo: Warsaw University of Technology, Warsaw, Poland
ep: Wayne State University, Detroit, Michigan, United States
eq: Yale University, New Haven, Connecticut, United States
er: Yerevan Physics Institute, Yerevan, Armenia
es: Yildiz Technical University, Istanbul, Turkey
et: Yonsei University, Seoul, South Korea
eu: Zentrum für Technologietransfer und Telekommunikation (ZTT), Fachhochschule Worms, Worms, Germany
ev: Dipartimento di Fisica dell'Universita, Udine, Italy
ew: M.V.Lomonosov Moscow State University, D.V.Skobeltsyn Institute of Nuclear Physics, Moscow, Russia
ex: Vinvca Institute of Nuclear Sciences, Belgrade, Serbia

JHEP07(2012)116